# Erosion Risk Assessment Tool For Construction Sites

Final Report

Prepared by

Bruce N. Wilson, Aleksey Sheshukov and Reid Pulley
Department of Biosystems and Agricultural Engineering
University of Minnesota

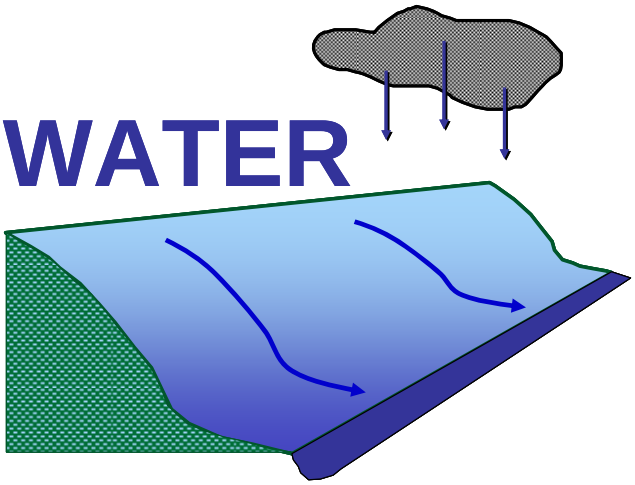


March, 2006

Published by
Minnesota Department of Transportation
Office of Research Administration
Mail Stop 330
395 John Ireland Boulevard
St. Paul, Minnesota 55155-1899

## *Funding Acknowledgement*

This project was conducted with funding provided by the Center for Transportation Studies (CTS) with financial resources and technical support of the Minnesota Department of Transportation (Mn/DOT.) The CTS supports the research mission of the University of Minnesota with a broad program covering many topics related to transportation. The program includes both fundamental and applied research, with the goal of expanding the existing body of transportation knowledge. In addition to providing financial support, Mn/DOT provided valuable input into the desired feature of the simulation tool

This project was also conducted with funding provided by the Minnesota Agricultural Experiment Station, Regional Projects S-1004.

## Technical Report Documentation Page

| 1. Report No. | 2. | 3. Recipients Accession No. |
|---|---|---|
| 4. Title and Subtitle<br>Erosion Risk Assessment Tool for Construction Sites | | 5. Report Date<br>April 2006<br>6. |
| 7. Author(s)<br>Bruce Wilson, Aleksey Sheshukov and Reid Pulley | | 8. Performing Organization Report No. |
| 9. Performing Organization Name and Address<br>Department of Biosystems and Agricultural Engineering<br>University of Minnesota<br>1390 Eckles Avenue<br>St. Paul, MN 55108 | | 10. Project/Task/Work Unit No.<br>11. Contract (C) or Grant (G) No. |
| 12. Sponsoring Organization Name and Address<br>Minnesota Department of Transportation<br>395 John Ireland Boulevard<br>St. Paul, Minnesota 55155 | | 13. Type of Report and Period Covered<br>Final Report<br>14. Sponsoring Agency Code |
| 15. Supplementary Notes | | |

16. Abstract (Limit: 200 words)

The impact of erosion and sediment from construction sites can be reduced by using a variety of onsite and offsite practices. The WATER model was developed to be a tool to assess the effectiveness of different sediment control practices. The WATER model evaluates risk by performing many simulations of a construction site response for different weather conditions. A particularly important component of the WATER model is the prediction of daily climate variables and storm characteristics called WINDS. This model uses the statistics for the analyzed data to predict many years of possible weather conditions. Predicted weather and storm characteristics are in very good agreement with those observed. The WATER model simulates surface runoff, plant processes, and erosion and sediment transport as major hillslope processes.

| 17. Document Analysis/Descriptors | | 18. Availability Statement | |
|---|---|---|---|
| Erosion Control<br>Best Management Practices<br>Risk Assessment<br>Simulation Model | | No restrictions. Document available from:<br>National Technical Information Services,<br>Springfield, Virginia 22161 | |
| 19. Security Class (this report)<br>Unclassified | 20. Security Class (this page)<br>Unclassified | 21. No. of Pages<br>148 | 22. Price |

# Erosion Risk-Protection Tool For Construction Sites

Final Report

Prepared by

Bruce N. Wilson, Ph.D.
Professor
Department of Biosystems & Agricultural Engineering
University of Minnesota

Aleksey Sheshukov, Ph.D.
Research Associate
Department of Biosystems & Agricultural Engineering
University of Minnesota

and

Reid Pulley
Graduate Student
Department of Biosystems & Agricultural Engineering
University of Minnesota

March, 2006

Published by
Minnesota Department of Transportation
Office of Research Administration
200 Ford Building Mail Stop 330
117 University Avenue
St. Paul, Minnesota 55155

.

## *Acknowledgements*

The authors appreciate the support of the Office of Environmental Services of the Minnesota Department of Transportation for this research and are indebted to Mr. Leo Holm and Mr. Dwayne Stenlund for their valuable assistance and support. The support of a companion project funded by the Minnesota Local Road Research Board (LRRB) contributed to the success of the project. The authors sincerely appreciate their support.

The authors would also like to acknowledge several people whose work was instrumental to the completion of this study.

- Leo Holm and Dwayne Stenlund of Mn/DOT for their input of important features to include in the model and their willingness to share the needs of the construction industry with the authors.
- Technical advisory team members of Katie Benik, Matthew Wassman, Jennifer Hildebrand, Larry Berkland, and Keith Cherryholmes for input
- Dan Warzala of Mn/DOT for his assistance in administrating the project.

## *Executive Summary*

Sediment loads from construction sites can be much greater than those from agricultural lands. The development of sediment control plans is therefore important in reducing the potential environmental impact of construction activities. Urban planers and engineers have a plethora of choices of onsite and offsite sediment control measures. The Watershed Assessment Tool for Environment Risk (WATER) model was developed to be a tool to assess the effectiveness of different sediment control practices. The WATER model evaluates risk by performing many simulations of construction site erosion for possible weather scenarios.

A particularly important component of the WATER model is the prediction of daily weather and storm characteristics. This prediction is done using a stand alone sub-module called the WINDS (Weather Input for Nonpoint Data Simulations) model. The WINDS model has routines to determine the statistical parameters of daily climate variables as well as intra-storm characteristics. Data from more than 200 climate and 200 15-minute precipitation stations have been analyzed, and the results have been stored in convenient files that are available to users to predict weather at their construction sites. The WINDS model uses algorithms to predict weather with the same statistical characteristics as those observed. A particular important algorithm is the methodology used to predict storm hyetographs. The WINDS model also allows the user to incorporate 5-day forecast information into the predictions. Predicted weather and storm characteristics were compared to those observed and were found to be in very good agreement.

Many years of possible weather conditions can easily be obtained with the WINDS model. The WATER model then converts this weather information into predicted sediment losses from construction sites. The key processes for this conversion are processes related to surface runoff, plant growth and evapotranspiration, and erosion and sediment transport. Since there is no one best modeling approach for all sites, the WATER model allows the user to select different modeling algorithms for most of the processes. The modeling approaches range from largely empirical relationships to fundamental process-based models. The selection of the best model is dependent on the availability of parameters and conditions at the construction site.

## *Table of Contents*


Introduction ..... 1

Background Information ..... 1
Overview of Modeling Concepts ..... 1
Objectives of the Study ..... 4

Overview of the WATER Model ..... 5

Introduction ..... 5
Risk Assessment Framework ..... 5
Insights from Technical Advisory Team ..... 7

Modeling Algorithms of the WINDS Model ..... 11

Introduction ..... 11
Observed Weather Data Sets ..... 11
Daily Climate Variables ..... 11
Data Sets for Intra-Storm Characteristics ..... 14
Analysis of Weather Data ..... 15
Daily Climate Variables ..... 15
Intra-Storm Characteristics ..... 21
Prediction of Daily Climate Variables ..... 30
Introduction ..... 30
Uncorrelated Non-Precipitation Weather Variables ..... 31
Correlated Non-Precipitation Variables ..... 32
Prediction of Storm Characteristics ..... 40
Theoretical Framework ..... 40
Storm Duration ..... 46
Fraction of Storm Duration with No Precipitation ..... 46
Additional Features ..... 49

Modeling Algorithms of the WATER Model ..... 51

Introduction ..... 51
Runoff Processes ..... 52
Infiltration and Surface Depressional Storage ..... 53
Overland Flow ..... 55
Plant Processes ..... 57
Plant Growth Modeling ..... 57
Evapotranspiration ..... 61
Erosion and Sediment Transport ..... 65
USLE-based Routines ..... 65
WEPP-based Routines ..... 66
University of Minnesota's Algorithms ..... 66

Summary and Conclusions ..... 68

## *List of Figures*

Figure 2.1.Risk Assessment Approach. ..... 6
Figure 2.2 Cumulative Probabilities for Different Sediment Control Strategies. ..... 7
Figure 2.3.Important Tasks Conducted at Construction Activities..... 9
Figure 2.4.Interface Window for the WINDS model. ..... 10
Figure 3.1.Locations of Daily Climate Stations Used in the WINDS model.. ..... 12
Figure 3.2.Location of Precipitation Stations Used in the WINDS Model. ..... 15
Figure 3.3.Trends in Normalized Means and Standard Deviation for Maximum Temperature... 18
Figure 3.4.Trends in Mean and Standard Deviations in Daily Precipitation Depth. ..... 20
Figure 3.5.Storm Duration as a Function of Precipitation Depth for Spring Valley, MN..... 22
Figure 3.6.Fraction of Time with No Precipitation for Storms At Spring Valley, MN..... 24
Figure 3.7.DDF values and Fitted Function for Holyoke, MN..... 29
Figure 3.8.Hypothetical Time Series of Temperature and Rainfall Intensity..... 31
Figure 3.9 Predicted Statistical Characteristics of Maximum Temperature at Rochester, MN.... 36
Figure 3.10.Predicted Statistical Characteristics of Maximum Relative Humidity at Rochester, MN. 37
Figure 3.11. Cross Correlation Coefficients between Minimum Relative Humidity and Selected Weather Variables at Rochester, MN. ..... 38
Figure 3.12. Serial Correlation Coefficients between Dewpoint Temperature and Selected Weather Variables at Rochester, MN. ..... 39
Figure 3.13. Predicted Daily Precipitation Statistics for Rochester, MN. ..... 41
Figure 3.14. Predicted and Observed Annual Precipitation Depth and Number of Wet Days for Rochester, MN. ..... 41
Figure 3.15. Hyetographs Derived from DDF Curves..... 43
Figure 3.16. Impact of No-Precipitation Gap on Intensity. ..... 48
Figure 3.17. Changes in Transitional Probabilities within Storms. ..... 49
Figure 4.1. Important Hillslope Processes for the WATER model. ..... 52
Figure 4.3. Relationship between Biomass and Photosynthetic Active Radiation. ..... 59
Figure 4.4 Plant Stress as Function of Air Temperature..... 60
Figure 4.5. Computations for a Community of Plant Groups..... 60
Figure 4.6. Energy Balance for Plant Canopy. ..... 62
Figure 4.7. Potential Transpiration Ratio as Function of Leaf Area Index..... 63
Figure 4.8. Leaf Resistance as Function of Leaf Potential. ..... 64

## *List of Tables*

Table 3.1. List of Daily Weather Variables for Minneapolis, MN. ..... 12
Table 3.2. Format of Climate Data File for Rochester, MN. ..... 13
Table 3.3. Format of the Precipitation Data File. ..... 16

# *Chapter 1*
# *Introduction*

## Background Information

Sediment loads from construction sites can be much greater than those from agricultural lands (Gray and Sotir, 1996). The development of sediment control plans is therefore important in reducing the potential environmental impact of construction activities. Urban planers and engineers have a plethora of choices of onsite and offsite sediment control measures. Choices for onsite control include mulches, erosion control blankets, vegetative sod and infiltration-enhancing practices. Detention ponds, infiltration basins, bioretention cells, and vegetative buffers are examples of offsite sediment control practices.

Different sediment control strategies are conveniently evaluated using simulation models. Current models typically predict erosion and sediment transport using concepts originally developed for agricultural landscapes. This approach presumes similar fundamental processes between the two different land uses that can be represented by the proper selection of parameters. New and innovative predictive techniques for sediment control practices are likely necessary to meet the needs of the construction sector.

Minnesota Department of Transportation (Mn/DOT) and the Minnesota Local Roads Research Board (LRRB) have provided funds to the principal investigator to study the usefulness of erosion control blankets and to explore fundamental detachment process. Extrapolating this information to the myriad of construction conditions in Minnesota requires a theoretical framework that links together the many factors influencing erosion. One important factor is highly variable weather conditions.

## Overview of Modeling Concepts

Scale is an important issue in the development and use of models. Different definitions of scale can be found in the literature. It will defined here as a time duration or length

dimension corresponding to a process, an observation or a model. Process-based models can be grouped by the scale at which they represent processes. Rigorous models typically represent processes at a relatively small scale. The overall response of a larger system is then obtained by linking the results from these small-scale processes. Parameters with this approach are considered to be fundamentally-based and therefore applicable to a wider range of problems. An example of an erosion model at the fine scale is the detachment model of Wilson (1993). Here the turbulent detachment forces acting on individual particles are considered in the erosion process.

Rigorous modeling approaches often are faced with estimating parameters from observed data that are gathered a different scale than the model. Interpretation of parameter values then becomes more difficult. Additional problems also emerge with the linking of many small scale processes for nonlinear systems. For such systems, relatively small errors at the process level grow resulting in poor predictions of the overall system. An alternative to predicting small-scale processes is to develop models corresponding to the observational or the decision-making scale of interest to the user. The framework and parameters for this approach are for the cumulative impact of complex small-scale processes. The use of this type of larger scale model to other applications is only appropriate if interactions among small-scale processes for these new applications are similar to the original data set. The Universal Soil Loss Equation (Wischmeier and Smith, 1965) is an example of an erosion model developed at the observational scale of the erosion plots from which the parameters are defined. The erodibility parameter here includes the integration of small-scale processes affecting particle detachment as well as those processes affecting infiltration.

The uniformity of model complexity among different components is another important consideration in model development. The “uniform slop” approach uses the same level of complexity for all components of the model. The overall accuracy of the model is inherently assumed to be determined by the accuracy of the weakest component. A rigorous representation of a process is not warranted when its input comes from a crudely represented component, succinctly captured by the adage “garbage in, garbage out”. An alternative to this philosophy is, however, appropriate if the response or management decisions are

particularly sensitive to one of the components. Greater effort in modeling that component may then be the best approach.

The availability of model parameters and the model sensitivity to potential error in these parameters are also important factors in the selection of modeling algorithms. Insight into the role of these two factors can be obtained from a first-order analysis for independent parameters. The uncertainty in predictions is defined as (Garen and Burges, 1981)

$$Var(\eta) = \sum_{i=1}^{n} S_i \, VAR(b_i) \tag{1.1}$$

where $\eta$ is the model result, $b_i$'s are model parameters, $S_i$ is the sensitivity coefficient for parameter $b_i$, $VAR(b_i)$ is the variance of the parameters and n is the number of parameters. The sensitivity coefficient is defined as the change in model results per change in parameter value.

The importance of parameter selection can be explored using Equation 1.1. A large variance reflects large uncertainty in predicted results and corresponds to a lack of confidence in drawing conclusion from simulated results. From Equation 1.1, confidence in predicted values is dependent on small variances (uncertainty) of parameters, small sensitivity coefficients, and/or small number of parameters. Rigorous models inevitably have more parameters than simple models. To have the same level of confidence, the sensitivity coefficients and/or the uncertainty of the parameters must then be reduced when using a more rigorous model to compensate for a larger n in Equation 1.1.

To summarize, the selection of models is dependent on the ability of the user to determine parameter values and the rigor of representing important processes. Although rigorous models are intellectually appealing for representing processes, they typically have many parameters that are frequently unknown. Application to a particular site is then difficult. In contrast, simple models of erosion have only a few parameters, but these parameters are likely derived from agricultural data. In addition, simple models do not capture important components of erosion and sediment transport. They are then unable to adequately assess the effectiveness of alternative sediment control practices. Models for construction sites

therefore need to have parameters that can be determined for site conditions and also be sufficiently rigorous to allow sediment control practices to be evaluated.

## Objectives of the Study

The overall goal of the proposed study is to develop a risk assessment tool for erosion from construction sites. Risk assessment is based on the impact of possible weather conditions on the effectiveness of different erosion control strategies. The specific research objectives are:

(1) To assess the needs and demands of erosion control practitioners working with construction projects
(2) To develop a simulation tool that allows practitioners to evaluate the risk of erosion on construction sites and that has a suitable framework to allow for easy expansion to meet the future needs of the road construction industry, and
(3) To evaluate the usefulness of the simulation tool using the experiences of seasoned erosion control professionals.

The general framework of the model is given in Chapter 2. This includes information received from erosion control practitioners by Objective 1. A description of the important sub-module to predict weather scenario is given in Chapter 3. The modeling approach used for hillslope processes is given in Chapter 4. An overall summary and conclusions are given in the final chapter.

# *Chapter 2*
# *Overview of the WATER Model*

## Introduction

The simulation tool for risk assessment is called the Watershed Assessment Tool for Environmental Risk (WATER) model. An overview of the modeling approach in the WATER model is given in this chapter. Of particular interest is the framework for assessing risk for variable weather conditions. Feedback from the advisory panel is also given in this chapter.

Details of the particular modeling algorithms of hillslope processes in the WATER model are given in Chapter 4. Since uncertainty in weather is of critical importance in assessing risk, the accurate prediction of possible weather scenarios is the foundation for the successful use of the WATER model. Algorithms for the prediction of weather have been combined into a stand alone climate generator called the WINDS (Weather Input for Nonpoint Data Simulations) model. Details of the algorithms used in the WINDS model are given in Chapter 3. Both WATER and WINDS models are written using Microsoft Visual C++ computer language.

## Risk Assessment Framework

The WATER model is designed to evaluate the risk associated with different sediment control measures. Risk assessment has historically been based on return periods associated with rainfall events. Although useful, this approach only considers the probability of a rainfall event; that is, it does not directly incorporate dynamic site conditions. The erosion model considers both the uncertainty of rainfall events and variability of conditions at construction sites.

The modeling approach of the risk assessment model is conceptually similar to that of the Water Erosion Prediction Project model (Flanagan and Nearing. 1995). With the WEPP

model, a climate generator is used to simulate many years of weather realization and corresponding soil erosion. The model was originally developed for agricultural lands. The average annual soil loss predicted by the WEPP model could be used, instead of Universal Soil Loss Equation, to select the best management practices.

The risk assessment approach of the WATER model is shown in Figure 2.1. Observed time series of maximum daily temperature at Duluth, Minnesota, USA for 1948, 1949 and 1991 are shown to illustrate the natural variability in yearly weather conditions. Also shown in Figure 2.1 is a hypothetical date for site disturbance by construction activities. Straw mulch and a silt fence are being considered as possible sediment control measures. The dates for the application/installation of these measures are also shown in Figure 2.1. Potential vegetal growth at the site is an important factor in modeling erosion.

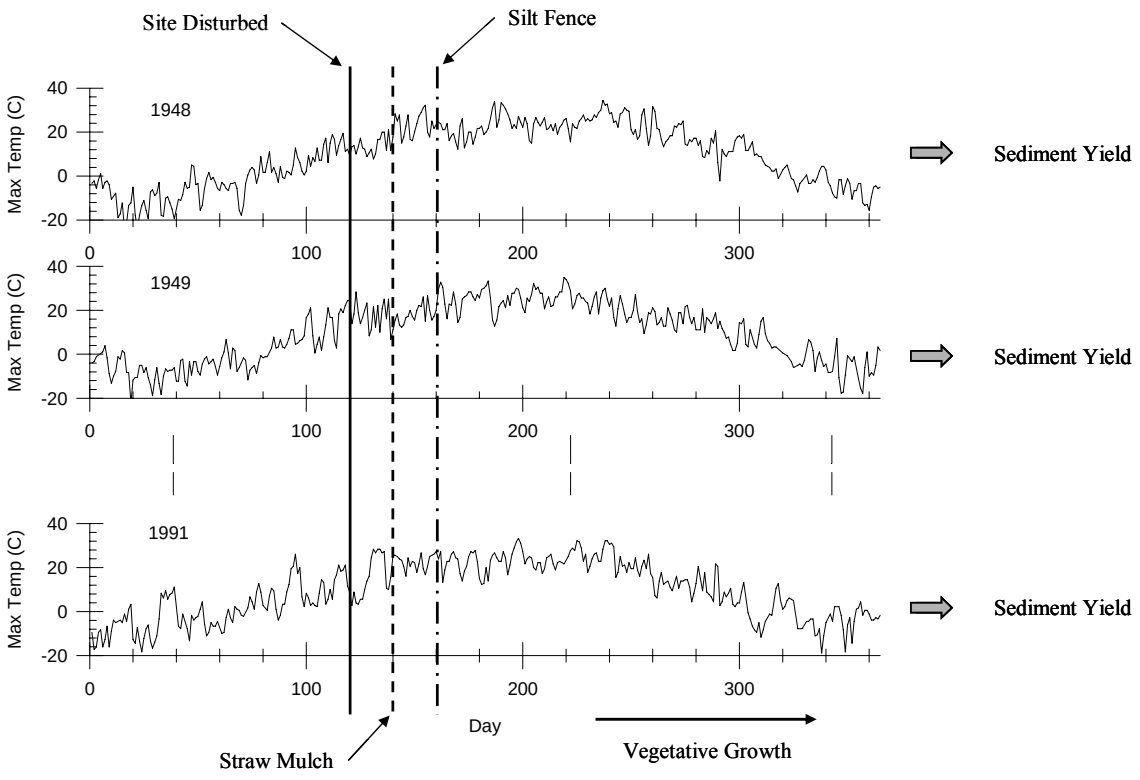


Figure 2.1. Risk Assessment Approach.

Risk assessment is done in the WATER model by simulating plant growth, runoff, and

erosion at the site after the start of construction activities. These processes are weather dependent and different responses are obtained for each yearly realization. Total sediment yield is obtained by summing the sediment yield for individual storms occurring after site disturbance. This process is repeated for different sediment control practices for each year of possible weather conditions. If a large number of realizations are used, probabilistic analyses of sediment yield data are possible. Hypothetical results for the straw mulch and silt fence scenarios are shown in Figure 2.2 using cumulative probabilities. If the user has an acceptable sediment loss goal, then the fraction of years that have yields less than or equal to the goal can be determined for each of the scenarios. This concept is illustrated in Figure 2.2.

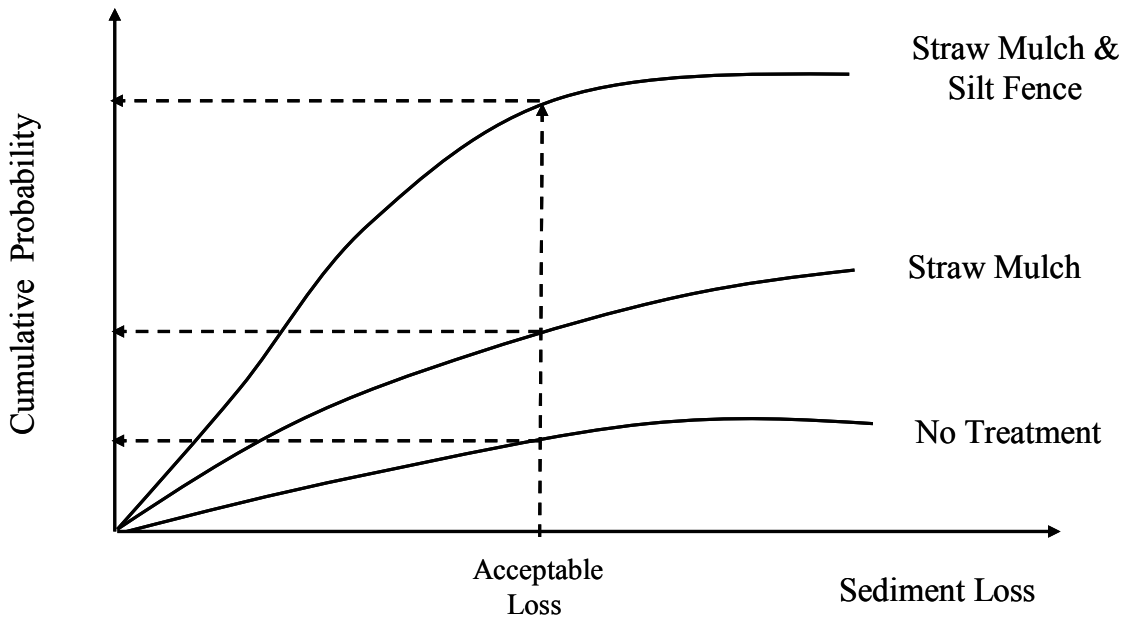


Figure 2.2 Cumulative Probabilities for Different Sediment Control Strategies.

Clearly the above approach is dependent on a good technique for determining the yearly weather conditions. Much of the work for the WATER model was in the development in unique algorithms to simulate the weather conditions. These algorithms are discussed in the next chapter.

## Insights from Technical Advisory Team

The needs and demands of erosion-control practitioners were assessed by seeking input from

a team of experienced erosion-control professionals. The advisory team members are Ms. Katie Benik, Environmental Services, Mn/DOT; Mr. Leo Holm, Environmental Services, Mn/DOT; Mr. Matthew Wassman, TKDA Consultants; Ms. Jennifer Hildebrand, Bonestroo, Rosene, Anderlik & Associates; Mr. Larry Berkland, Steele County and Dr. Keith Cherryholmes, Minnesota Pollution Control Agency.

As part of brainstorming activities, the team suggested the following erosion/sediment control practices for consideration in the WATER model development: straw mulch, wood chips, sod, straw and wood blankets, temporary seeding, surface roughening, hydraulically applied mulches, soil stabilizers, long-term seeding-vegetation, silt fences, diversions created by straw waddles, bundles, biorolls, triangular silt dikes, composite material, pond, infiltration basins, vortex swirls, rock checks, inlet protection, hard concrete armament, porous pavement, and bioengineering methods. The advisory team understood that implementation of all of these practices exceeded the scope of the project. Selection of practices was left to discretion of the principal investigator.

The advisory team also discussed important site information for the proper design of erosion/sediment control practices. They were summarized into the following categories: soil type (clay, silt loam, sand), slope gradient and aspect, soil compaction, topsoil and subsoil, surrounding topography for runon impacts and existing vegetation. The team identified the specification of construction time lines as major issue in developing a construction site model. Timelines are dependent on unknown weather conditions and can vary greatly with contractors and subcontractors. A summary of important construction activities is shown in Figure 2.3.

The technical advisory team for the project identified having a user friendly interface as important. An example of the interface for the WINDS model is shown in Figure 2.4. Drop down menu options are used and are consistent with those used by most commercial software packages. The user is guided through the myriad of features available in the WINDS and WATER models using a “wizard”. The user can opt for the basic (default) option for input or for the advanced option. The basic option has a minimum number of inputs. The

advanced option allows the user to tailor the simulation approach to the particular characteristics of the site and his/her expertise.

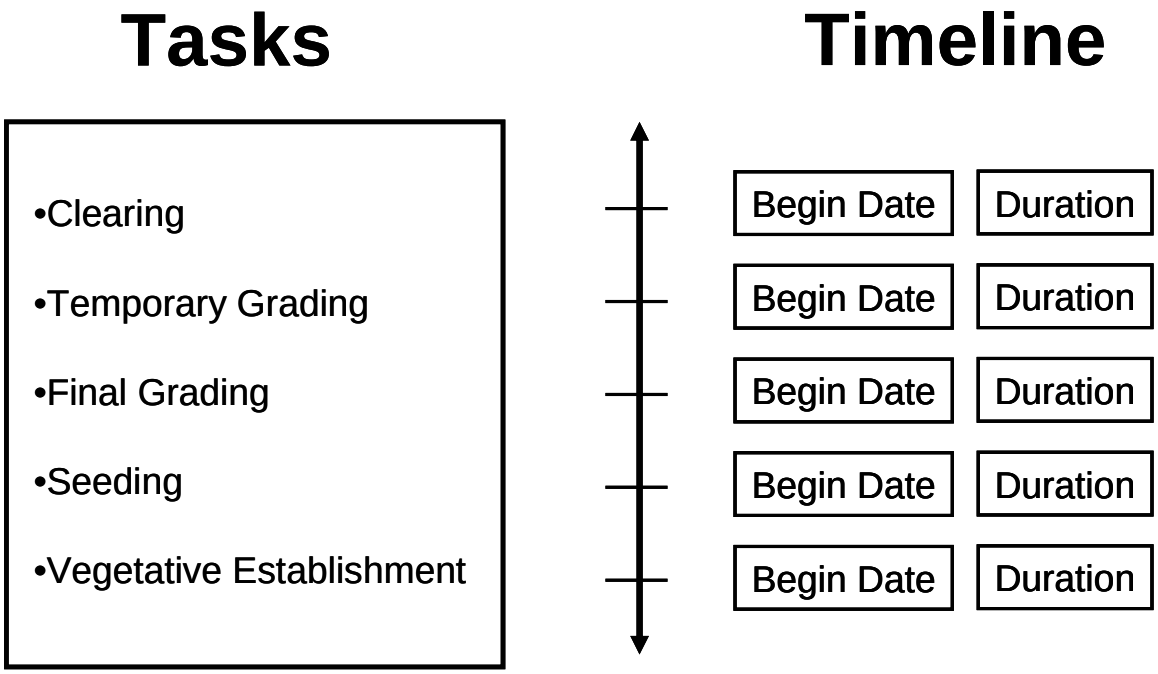


Figure 2.3. Important Tasks Conducted at Construction Activities.

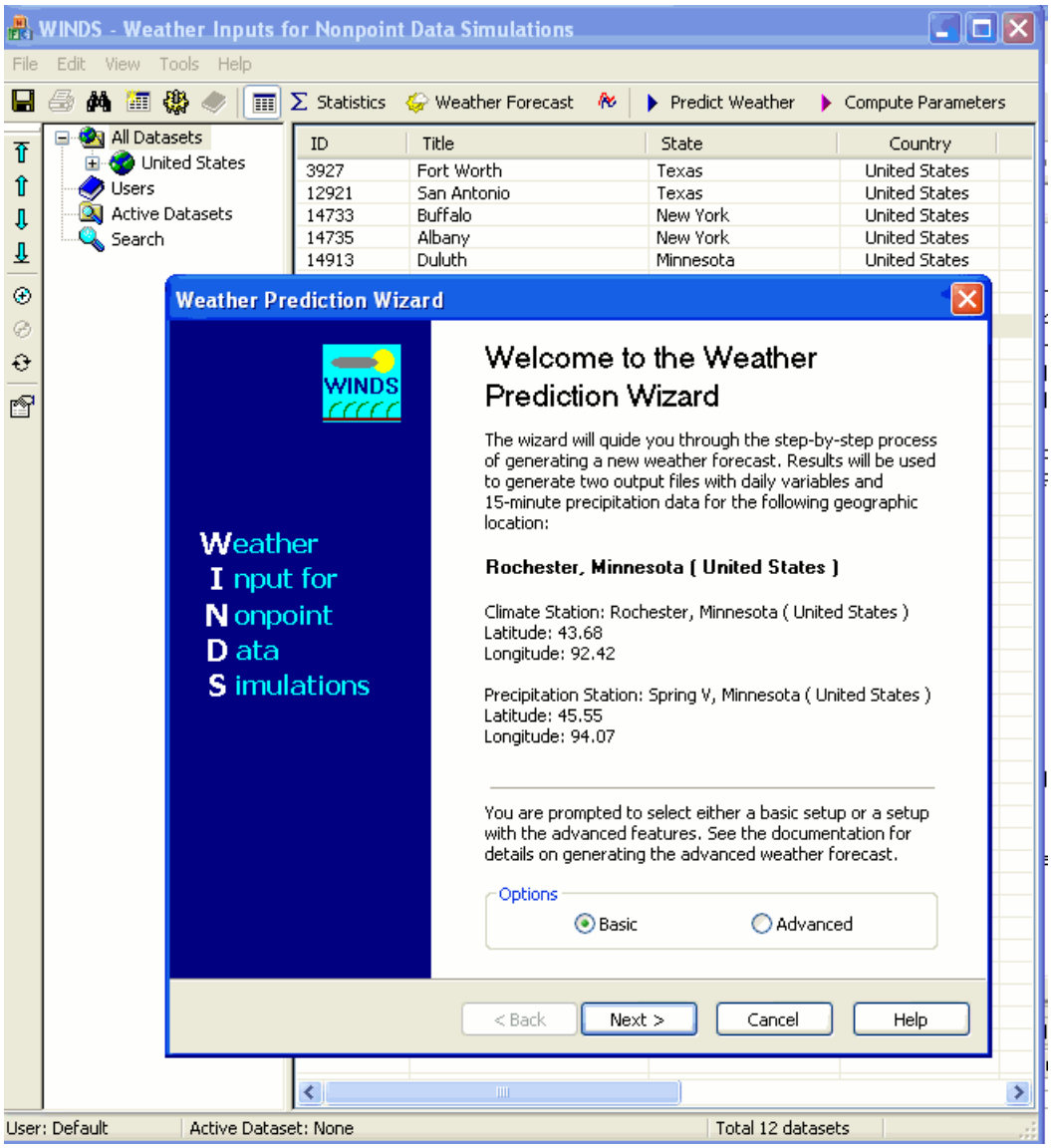


Figure 2.4. Interface Window for the WINDS model.

# *Chapter Three*
# *Modeling Algorithms of the WINDS Model*

## Introduction

Climate generators allow many years of possible weather scenarios to be used to determine the characteristics of runoff and sediment. Useful climate generators are developed in two stages. First, the historic weather records are analyzed to obtain pertinent statistical information. Since these characteristics vary with day of year, daily or monthly ensemble statistics are typically used to capture seasonal trends. Second, statistical methods are developed and implemented to use the observed statistical information to predict time series of weather variables.

The description of the WINDS model is divided into five sections. The first section describes the observed weather data sets used to determine the parameters for the WINDS model. The second section describes the algorithms for analyzing these data sets. The next two sections are then used to describe the predictive algorithms of the WINDS model. Separate sections are used to describe algorithms for daily climate variables and for storm characteristics. The last section is used to describe special features of the WINDS model.

## Observed Weather Data Sets

### *Daily Climate Variables*

Statistical characteristics of daily climate variables were computed from two different types of data sets. Data from the National Climatic Data Center (NCDC) and from the Solar and Meteorological Surface Observational Network (SAMSON) were used to obtain daily weather records for 208 climate stations. The location of these stations is shown in Figure 3.1. A summary of the daily weather variables evaluated at each of these stations is given in Table 3.1. The length of the data record varied with individual variables, as shown in Table 3.1 for the Minneapolis site. The longest record length for any particular weather variable among all climate stations was 129 years, and the shortest record length was 28 years.

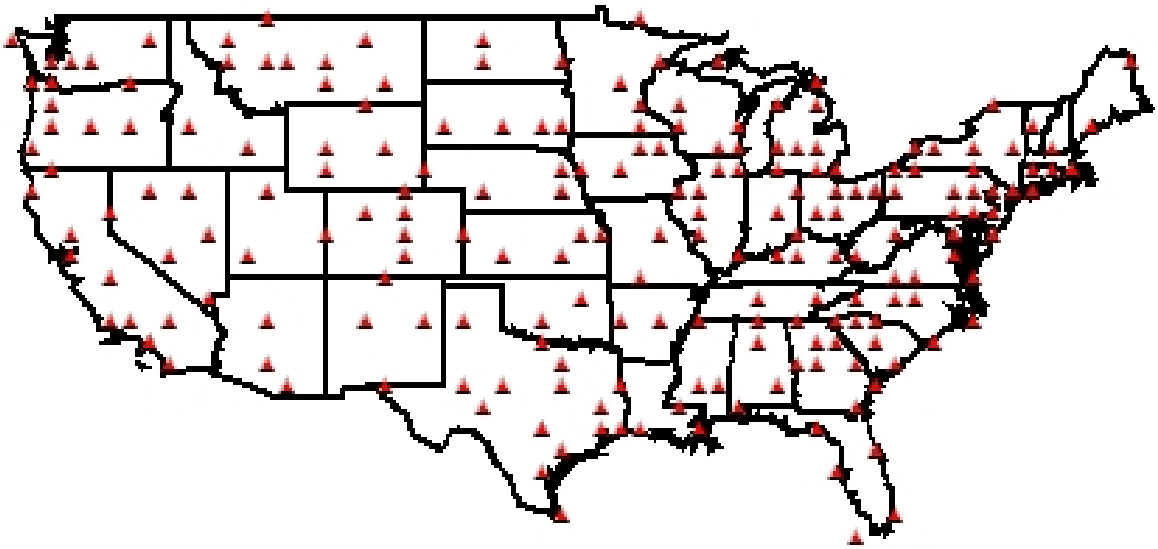

Figure 3.1. Locations of Daily Climate Stations Used in the WINDS model.

Table 3.1. List of Daily Weather Variables for Minneapolis, MN.

| Variables | Units | Symbol | Length (Years) | From (Month-Year) | To (Month-Year) |
|---|---|---|---|---|---|
| Temperature, Max | °C | TMAX | 103 | Jan-1891 | Dec-2003 |
| Temperature, Min | °C | TMIN | 103 | Jan-1891 | Dec-2003 |
| Relative Humidity, Max | % | RHMAX | 56 | Jul-1948 | Dec-2003 |
| Relative Humidity, Min | % | RHMIN | 56 | Jul-1948 | Dec-2003 |
| Dew Point Temperature | °C | DPTP | 43 | Jan-1961 | Dec-2003 |
| Ave Wind Speed | m/s | AVWD | 43 | Jan-1961 | Dec-2003 |
| Max Wind Speed | m/s | PKWND | 36 | Jan-1961 | May-1996 |
| Wind Direction | deg | WINDIR | 43 | Jan-1961 | Dec-2003 |
| Atmospheric Pressure | kPa | PRESS | 43 | Jan-1961 | Dec-2003 |
| Solar Radiation | $MJ/m^2$ | RAD | 40 | Jan-1961 | Dec-2000 |
| Precipitation | mm | PRCP | 103 | Jan-1891 | Dec-2003 |

The NCDS and SAMSON data sets were combined into a single input file. This combined data set was used to compute the statistical characteristics. The format used in the input file is shown in Table 3.2. The definition of the header variables are given in Table 3.1. Missing values were represented by "999999". Missing values were not used in the computation of statistics. Percent sunshine and Julian day were also created in the combined data file. However, a statistical analysis of percent sunshine was not done as part of this project.

Table 3.2. Format of Climate Data File for Rochester, MN.

| YEAR | MONTH | DAY | TMAX | TMIN | PRCP | RHMAX | RHMIN | DPTP | AVWD | PKWND | WINDIR | PRESS | PSUN | RAD | JULIAN |
|---|---|---|---|---|---|---|---|---|---|---|---|---|---|---|---|
| 1928 | 10 | 1 | 21.67 | 7.78 | 999999 | 999999 | 999999 | 999999 | 999999 | 999999 | 999999 | 999999 | 999999 | 999999 | 275 |
| 1928 | 10 | 2 | 16.11 | -1.11 | 999999 | 999999 | 999999 | 999999 | 999999 | 999999 | 999999 | 999999 | 999999 | 999999 | 276 |
| 1928 | 10 | 3 | 21.11 | 5 | 999999 | 999999 | 999999 | 999999 | 999999 | 999999 | 999999 | 999999 | 999999 | 999999 | 277 |
| 1928 | 10 | 4 | 25 | 13.33 | 4 | 999999 | 999999 | 999999 | 999999 | 999999 | 999999 | 999999 | 999999 | 999999 | 278 |
| 1928 | 10 | 5 | 21.11 | 4.44 | 999999 | 999999 | 999999 | 999999 | 999999 | 999999 | 999999 | 999999 | 999999 | 999999 | 279 |
| 1928 | 10 | 6 | 18.89 | 8.33 | 999999 | 999999 | 999999 | 999999 | 999999 | 999999 | 999999 | 999999 | 999999 | 999999 | 280 |
| 1928 | 10 | 7 | 20.56 | -1.11 | 999999 | 999999 | 999999 | 999999 | 999999 | 999999 | 999999 | 999999 | 999999 | 999999 | 281 |
| 1928 | 10 | 8 | 24.44 | 6.11 | 999999 | 999999 | 999999 | 999999 | 999999 | 999999 | 999999 | 999999 | 999999 | 999999 | 282 |
| 1928 | 10 | 9 | 23.89 | 5.56 | 999999 | 999999 | 999999 | 999999 | 999999 | 999999 | 999999 | 999999 | 999999 | 999999 | 283 |
| 1928 | 10 | 10 | 19.44 | 999999 | 999999 | 999999 | 999999 | 999999 | 999999 | 999999 | 999999 | 999999 | 999999 | 999999 | 284 |
| 1928 | 10 | 11 | 13.33 | 18.33 | 999999 | 999999 | 999999 | 999999 | 999999 | 999999 | 999999 | 999999 | 999999 | 999999 | 285 |
| 1928 | 10 | 12 | 999999 | 11.67 | 13 | 999999 | 999999 | 999999 | 999999 | 999999 | 999999 | 999999 | 999999 | 999999 | 286 |
| 1928 | 10 | 13 | 999999 | 4.44 | 1 | 999999 | 999999 | 999999 | 999999 | 999999 | 999999 | 999999 | 999999 | 999999 | 287 |
| 1928 | 10 | 14 | 9.44 | 5 | 999999 | 999999 | 999999 | 999999 | 999999 | 999999 | 999999 | 999999 | 999999 | 999999 | 288 |
| 1928 | 10 | 15 | 18.89 | 8.89 | 999999 | 999999 | 999999 | 999999 | 999999 | 999999 | 999999 | 999999 | 999999 | 999999 | 289 |
| 1928 | 10 | 16 | 18.33 | 14.44 | 18 | 999999 | 999999 | 999999 | 999999 | 999999 | 999999 | 999999 | 999999 | 999999 | 290 |
| 1928 | 10 | 17 | 17.22 | 6.67 | 0 | 999999 | 999999 | 999999 | 999999 | 999999 | 999999 | 999999 | 999999 | 999999 | 291 |
| 1928 | 10 | 18 | 8.33 | 6.67 | 17 | 999999 | 999999 | 999999 | 999999 | 999999 | 999999 | 999999 | 999999 | 999999 | 292 |
| 1928 | 10 | 19 | 10.56 | 999999 | 3 | 999999 | 999999 | 999999 | 999999 | 999999 | 999999 | 999999 | 999999 | 999999 | 293 |
| 1928 | 10 | 20 | 9.44 | 999999 | 999999 | 999999 | 999999 | 999999 | 999999 | 999999 | 999999 | 999999 | 999999 | 999999 | 294 |
| 1928 | 10 | 21 | 16.11 | 999999 | 999999 | 999999 | 999999 | 999999 | 999999 | 999999 | 999999 | 999999 | 999999 | 999999 | 295 |
| 1928 | 10 | 22 | 17.22 | 1.11 | 999999 | 999999 | 999999 | 999999 | 999999 | 999999 | 999999 | 999999 | 999999 | 999999 | 296 |
| 1928 | 10 | 23 | 10 | 0.56 | 999999 | 999999 | 999999 | 999999 | 999999 | 999999 | 999999 | 999999 | 999999 | 999999 | 297 |
| 1928 | 10 | 24 | 15 | 999999 | 999999 | 999999 | 999999 | 999999 | 999999 | 999999 | 999999 | 999999 | 999999 | 999999 | 298 |
| 1928 | 10 | 25 | 11.11 | -1.11 | 999999 | 999999 | 999999 | 999999 | 999999 | 999999 | 999999 | 999999 | 999999 | 999999 | 299 |
| 1928 | 10 | 26 | 10 | -4.44 | 999999 | 999999 | 999999 | 999999 | 999999 | 999999 | 999999 | 999999 | 999999 | 999999 | 300 |
| 1928 | 10 | 27 | 11.11 | 0 | 999999 | 999999 | 999999 | 999999 | 999999 | 999999 | 999999 | 999999 | 999999 | 999999 | 301 |
| 1928 | 10 | 28 | 7.78 | 0.56 | 999999 | 999999 | 999999 | 999999 | 999999 | 999999 | 999999 | 999999 | 999999 | 999999 | 302 |
| 1928 | 10 | 29 | 3.89 | -9.44 | 999999 | 999999 | 999999 | 999999 | 999999 | 999999 | 999999 | 999999 | 999999 | 999999 | 303 |
| 1928 | 10 | 30 | 4.44 | -8.89 | 999999 | 999999 | 999999 | 999999 | 999999 | 999999 | 999999 | 999999 | 999999 | 999999 | 304 |
| 1928 | 10 | 31 | 8.33 | 2.78 | 999999 | 999999 | 999999 | 999999 | 999999 | 999999 | 999999 | 999999 | 999999 | 999999 | 305 |

Radiation data are converted into the ratio of that measured at the station to a theoretical value that would be obtained when the earth's atmospheric effects are negligible. The theoretical value is defined as (Lee, 1978)

$$R_a = (\frac{1440}{\pi})\, S_c \cos(\frac{lat\ \pi}{180}) \cos(\phi)[\sin(\omega_s) - \omega_s \cos(\omega_s)\,] \tag{3.1}$$

where $R_a$ is the radiation at the station without any atmospheric effects, lat is the station latitude, $S_c$ is the solar flux density, $\phi$ is the solar declination angle, and $\omega_s$ is the sunset hour angle. Relationships to estimate these values are shown below.

$$S_c = \frac{1.95\,(1 + 0.033\cos(2\pi\, day / 365))}{24} \tag{3.2a}$$

$$\phi = 0.4093 \sin\left(\frac{2\,\pi\,(284 + day)}{365}\right) \tag{3.2b}$$

$$\omega_s = \arccos\left(-\tan\left(\frac{lat\,\pi}{180}\right)\tan(\phi)\right) \tag{3.2c}$$

Statistical characteristics for radiation are done using the radiation ratio defined as

$$RAD^* = \frac{RAD}{R_a} \tag{3.3}$$

In prediction radiation, the $RAD^*$ is first computed. The RAD is then obtained by multiplying this value by the theoretical value given by Equation 3.2. The theoretical value only requires day of the year and the latitude of the construction site.

*Data Sets for Intra-Storm Characteristics*

The NCDS and SAMSON data sets are used to determine statistical characteristics to predict the daily climate variables, including the total depth of precipitation for each storm. In addition to the weather condition represented by these values, the intra-storm characteristics are also needed for accurate simulation of hillslope runoff and erosion processes. Of particular interests for the WINDS model are the storm duration, the fraction of total duration with no precipitation, transitional probabilities between rain and no-rain bursts, and the distribution of intensities within storm (i.e., hyetograph).

Intra-storm characteristics were computed from data sets of 15-minute precipitation depths purchased from Hydrosphere Data Products located in Boulder, Colorado. For each of NCDC/SAMSON climate station, a nearby precipitation station was selected. Therefore, 208 precipitation stations were chosen for analysis of intra-storm characteristics. The locations of these stations are shown in Figure 3.2. The length of record at precipitation stations was considerably shorter than the climate stations data. The average record length for all stations was 26 years.

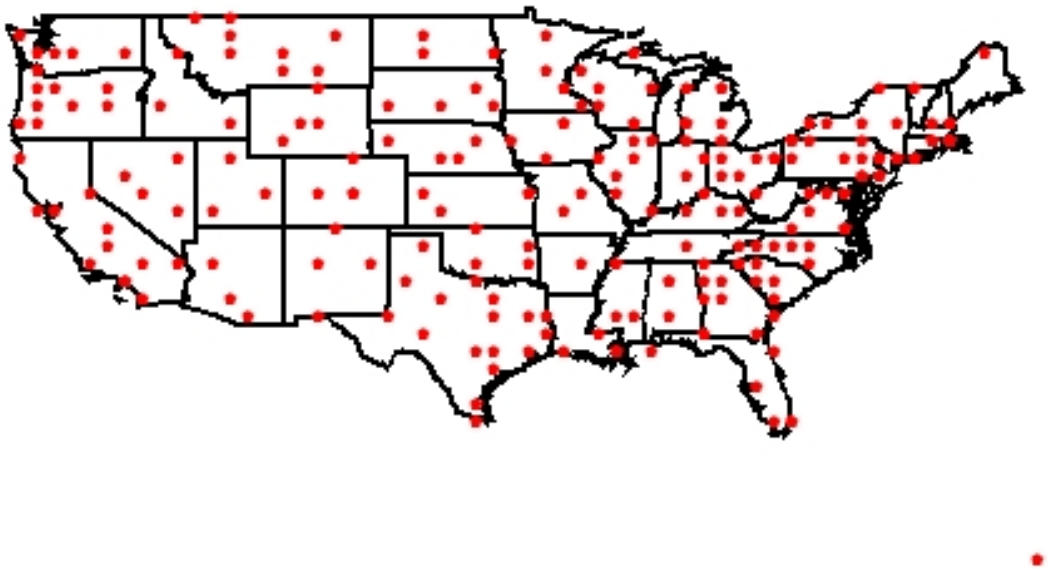

Figure 3.2. Location of Precipitation Stations Used in the WINDS Model.

The format of the data files for the precipitation stations is shown in Table 3.3. The start of each year had the same header information. Precipitation depths were recorded for each 15 minute increment starting at 1 am and ending at 1 am the next day. The total precipitation depth is given in the last column. All precipitation depths were converted into millimeters. Missing data were represented by the code "—M" or "—D". The notation of "—A" indicated that only the cumulated depth was recorded over the intervals with this notation. The cumulated depth was divided equally for all 15 minute increments. Total storm duration was defined as the time interval between the first and last measured storm depths within each day. No attempts were made to evaluate whether the observed depths were caused by more than one storm.

## Analysis of Weather Data

### *Daily Climate Variables*

The WINDS model includes routines to compute the observed statistical characteristics of the NCDS/SAMSON daily climate files and the Hydrosphere intra-storm data files. A paired set of files are required to use these routines. The computer code of the analyses of historical data are organized in a class called CWindsParameters. Separate sections are used to

describe the algorithms used to determine the pertinent statistical characteristics of daily climate and the intra-storm records.

Table 3.3. Format of the Precipitation Data File.

| | | | |
|---|---|---|---|
| Station | SPRING VALLEY | Parameter | Prcp |
| County | FILLMORE | Record Cnt | 29 |
| State | MN | Coverage % | 87 |
| ID | 7941 | Latitude 43:41:00 | Begin Date 05/1971 |
| Elevation | 1275 | Longitude 092:25:00 | End Date 12/1999 |

1971

Quarter-Hourly Precipitation in Hundredths of an inch

| | 100 | 115 | 130 | 145 | 200 | 215 | ... | 2400 | 2415 | 2430 | 2445 | 2500 |
|---|---|---|---|---|---|---|---|---|---|---|---|---|
| 1/1/1971 | 0 | 0 | 0 | 0 | 0 | 0 | ... | 0 | 0 | 0 | 0 | 0 |
| 1/2/1971 | 0 | 0 | 0 | 0 | 0 | 0 | ... | 0 | 0 | 0 | 0 | 0 |
| 1/3/1971 | 0 | 0 | 0 | 0 | 0 | 0 | ... | 0 | 0 | 0 | 0 | 0 |
| 1/4/1971 | 0 | 0 | 0 | 0 | 0 | 0 | ... | 0 | 0 | 0 | 0 | 0 |
| 1/5/1971 | 0 | 0 | 0 | 0 | 0 | 0 | ... | 0 | 0 | 0 | 0 | 0 |
| 1/6/1971 | 0 | 0 | 0 | 0 | 0 | 0 | ... | 0 | 0 | 0 | 0 | 0 |
| 1/7/1971 | 0 | 0 | 0 | 0 | 0 | 0 | ... | 0 | 0 | 0 | 0 | 0 |
| 1/8/1971 | 0 | 0 | 0 | 0 | 0 | 0 | ... | 0 | 0 | 0 | 0 | 0 |
| 1/9/1971 | 0 | 0 | 0 | 0 | 0 | 0 | ... | 0 | 0 | 0 | 0 | 0 |
| 1/10/1971 | 0 | 0 | 0 | 0 | 0 | 0 | ... | 0 | 0 | 0 | 0 | 0 |
| 1/11/1971 | 0 | 0 | 0 | 0 | 0 | 0 | ... | 0 | 0 | 0 | 0 | 0 |
| 1/12/1971 | 0 | 0 | 0 | 0 | 0 | 0 | ... | 0 | 0 | 0 | 0 | 0 |
| 1/13/1971 | 0 | 0 | 0 | 0 | 0 | 0 | ... | 0 | 0 | 0 | 0 | 0 |

For all non-precipitation data, the mean, standard deviation and skew coefficient are computed for the five-day intervals, and therefore, seventy-three values are used to represent trends within the year. The mean, standard deviation and skew coefficient for each five-day interval are defined as

$$E(x_j) = \frac{\sum_{i=1}^{n} x_{ji}}{n} \tag{3.4a}$$

$$STDEV(x_j) = \sqrt{\frac{\sum_{i=1}^{n} (x_{ji} - E(x_j))^2}{n-1}} = \sqrt{\frac{\sum_{i=1}^{n} x_{ji}^2 - (\sum_{i=1}^{n} x_{ji})(\sum_{i=1}^{n} x_{ji})/n}{n-1}} \tag{3.4b}$$

$$SKEW(x_j) = \frac{n\sum_{i=1}^{n} (x_{ji} - E(x_j))^3}{(n-1)(n-2)STDEV(x_j)} = \frac{n^2\sum_{i=1}^{n} x_{ji}^3 - 3n(\sum_{i=1}^{n} x_{ji})(\sum_{i=1}^{n} x_{ji\,ji}^2) + 2(\sum_{i=1}^{n} x_{ji})^3}{n\,(n-1)\,(n-2)\,STDEV(x_j)} \tag{3.4c}$$

where $x_j$ and n are the non-precipitation variable and the number of observation, respectively, for the jth five-day interval. Means and standard deviations are normalized by dividing the

values of Equations 3.4a and 3.4b by the yearly mean and yearly standard deviation, respectively. Normalized values allow the means and standard deviations to be summarized without using units. Other advantages are discussed later.

An output file of the observed statistical characteristics is created and is used as input to the WINDS model. The first lines of this file contain information about the station and yearly normalizing means and standard deviations. The variations in statistics within the year are represented by cosine functions with three different harmonics, as suggested by Richardson (1981). The general form of this function is:

$$STAT^{*}(x_j) = b_o + b_1 \cos(t_j + b_2) + b_3 \cos(2t_j + b_4) + b_5 \cos(3t_j + b_6) \tag{3.5}$$

where $STAT^{*}(x_j)$ is the normalized mean, normalized standard deviation, and skew coefficient, and where $t_j = 2(day_j)\pi/365$.

Initial estimates of the b coefficients of Equation 3.5 are obtained from the theory for harmonic analysis as given by Priestly (1981). Final estimates were taken by using a modified nonlinear Gauss method where the impact of adding higher order harmonics could be considered. This impact was assessed by first computing the residual sum of squares using the lowest-order harmonic. Higher order harmonics were added if the percent improvement in the residual sum of squares was greater than 0.1%. The normalized mean square error was saved in the climate parameter output file as a measure of the goodness of fit of the cosine curve.

An example of a cosine-fitted curve is shown in Figure 3.3 for the normalized mean and normalized standard deviation of maximum temperature for Rochester, Minnesota. The cosine function of Equation 3.5 was effective in capturing within-year trends in the daily means and standard deviations for this data set. Visual comparison of trends at other locations resulted in similar conclusions; that is, if there was a discernible observed trend, then the cosine function fit that trend well. A poor fit (no trends within a year) results in a relatively large normalized mean square error. In the prediction of weather variables by the WINDS model, a constant value is used throughout the entire year when the normalized mean square value is greater than 0.65. The constant value is the average of the type of data

shown in Figure 3.3.

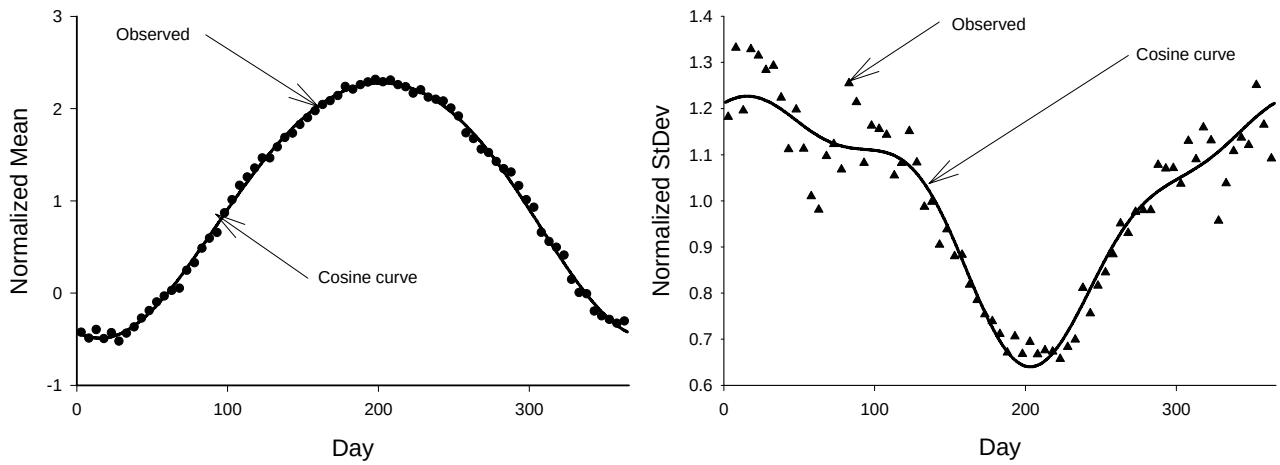


Figure 3.3. Trends in Normalized Means and Standard Deviation for Maximum Temperature.

Intuitively, if the maximum temperature for any given day is greater than its mean, then the minimum temperature would likely also be greater than its mean. This statistical property can be captured by using cross correlations. Likewise, if the maximum temperature for any given day is greater than its mean, then the maximum temperature of the next day would likely also be greater than its mean. This property can be captured using serial correlations. Cross correlation coefficients and serial correlation coefficients are computed by conducting a second pass through the climate data set and by using the following equations

$$COR(x_{pj}, x_{qj}) = \frac{\sum_{i=1}^{n} (x_{pji} - E(x_{pj}))\,(x_{qji} - E(x_{qj}))}{(n-1)\,STDEV(x_{pj})\,STDEV(x_{qj})} \tag{3.6a}$$

$$SCOR(x_{pj}, x_{qj-1}) = \frac{\sum_{i=1}^{n} (x_{pji} - E(x_{pj}))\,(x_{qj-1i} - E(x_{qj-1}))}{(n-1)\,STDEV(x_{pj})\,STDEV(x_{qj-1})} \tag{3.6b}$$

where p and q refers to specific non-precipitation daily variables as identified in Table 3.1.

The above equations are used to compute correlation correlations and serial correlation coefficients using a five-day interval (for a total of 73 intervals) for each of the summation terms. The matrix of correlation coefficients for each of these intervals is symmetrical, that

is, the correlation between maximum temperature and minimum temperature is the same as the correlation between minimum temperature and maximum temperature. However, the matrix of serial correlations coefficients is not necessarily symmetrical because the serial correlation between the current-day maximum temperature and the previous-day minimum temperature may not equal that between the current-day minimum temperature and previous-day maximum temperature. The consequence of a non-symmetrical matrix is that more coefficients are needed for serial correlation than for cross correlation. A non-normalized cosine function of Equation 3.5 was fitted to fifty-eight different cross correlation coefficients and one-hundred different serial correlation coefficients. The cosine coefficients are stored in the output data file and are once again used as input into the WINDS model.

The number of observation to compute the means, standard deviations, and skew coefficients of Equations 3.4 corresponds to all days within the five-day interval that had an observed value. Richardson (1981) suggested that these statistics are also dependent on whether there was precipitation on that day. To indirectly consider correlation between non-precipitation variables and precipitation, the statistics of Equations 3.4 were also computed for dry days only and wet days only, where wet days were defined as those days with measurable precipitation depth. Dry-days statistics were computed using Equations 3.4 with observations only from days with no precipitation. The appropriate summations for wet days were obtained by subtracting dry-days summation terms from those of the total (all days).

Daily precipitation depths were also analyzed to determine the mean, standard deviation and skew coefficient by using Equations 3.4. Since the number of observations for computing these statistics is typically much smaller than non-precipitation variables, a twenty-eight day averaging interval is used for daily precipitation characteristics. Within-year variations in statistics were once again represented by using coefficient for the fitted cosine function of Equation 3.5. Mean and standard deviation of daily precipitation depth were normalized by the station annual precipitation depth and the annual standard deviation. A plot of normalized mean and standard deviation with the fitted cosine curve is shown in Figure 3.4. The cosine curve was able to accurate capture within-year variations in the statistics. To provide greater flexibility in predicting the rainfall depth, the parameters of the generalized

extreme value distribution were also computed using twenty-eight-day intervals. This includes central tendency, spread, and skewness parameters. The harmonic cosine functions were used to represent within-year variations in these statistics.

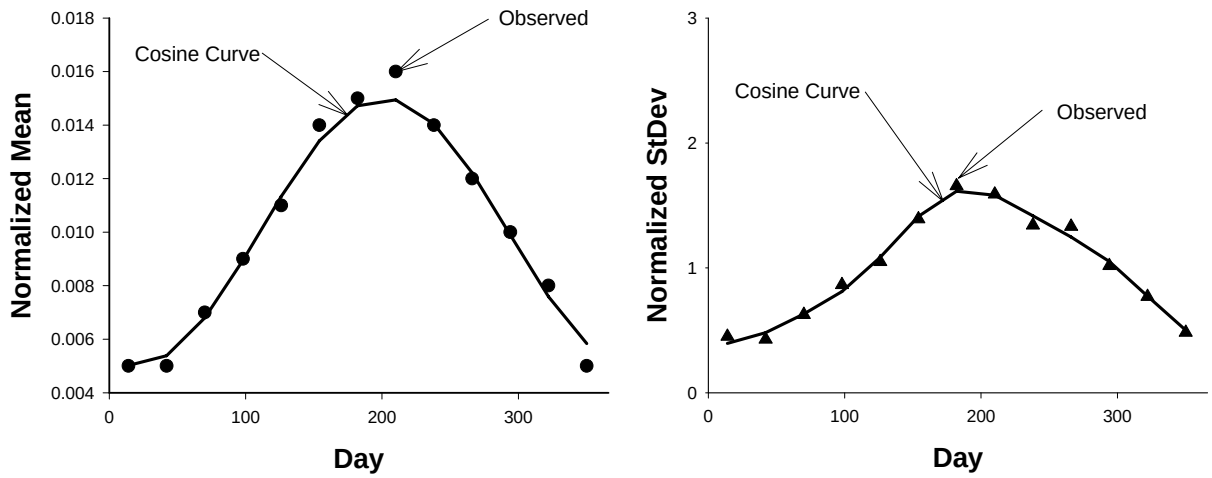


Figure 3.4. Trends in Mean and Standard Deviations in Daily Precipitation Depth.

Daily precipitation data were also used to compute the transitional probabilities of wet-to-wet days and dry-to-wet days. These transitional probabilities were obtained by counting the number of consecutive wet-wet and dry-wet days within twenty-eight day intervals. The probability of a wet day was also computed. Within year trends were represented by the cosine function. The total number of wet days was computed, as well as the average annual precipitation depth.

A frequency analysis of the daily depth was also done to determine the depths corresponding to return periods of 2 year, 5 year, 10 year, 25 year, 50 year and 100 year. This analysis required that the identification of the largest daily precipitation depth for each year, resulting in a maximum annual time series. Following widely used concepts first given by Hershfield (1961), this type of time series data was converted to a partial time series by multiplying the results obtained from the maximum annual time series by adjustment factors of 1.13, 1.04, and 1.01 for the 2-y, 5-y, and 10-y depths, respectively. Another issue is the difference in

precipitation depth between fixed 24-h period (as recorded in the data sets) and 24-h clock time that corresponds to storms that have precipitation in two fixed 24-h periods. Adjustments to account for differences between clock-time (actual storm duration) and daily precipitation depth were investigated by Hershfield (1961). Based on his work, the daily precipitation depth was multiplied by a factor of 1.13 to convert it to an equivalent clock-time depth.

Two different methods were used to estimate the depths corresponding to different return periods. For both approaches, the statistics are first obtained from the maximum annual time series with adjustments for daily to clock-hour values. One of the methods used the plotting position to estimate the depth corresponding to the two-year return period and the extreme value type I distribution to estimate the 100-year depth. Depths corresponding to the 5-y, 10-y, 25-y, and 50-y return periods were determined by interpolating between these two depths using relationships derived from the extreme value type I distribution. The other method used the generalized extreme value type distribution to estimate the return period depths. The derived parameters from the adjusted maximum annual time series were used to estimate depths for all of the return periods. The return-period depths obtained from both methods were adjusted to partial duration series as previously discussed. Return-period depths from the daily precipitation play an important role in the defining depth-duration-frequency curves discussed in the next section.

*Intra-Storm Characteristics*

In the CWindsParameter Class, a separate output data file is created to store the results of the statistical analyses of intra-storm characteristics. This output file becomes an input file for prediction of weather with the WINDS model. Possible within-year variations in statistics were computed using twenty-eight day intervals. A non-normalized cosine function of Equation 3.5 was again fitted to the data, and the coefficients are stored in the output data file. Similar to the analysis at the climate stations, the daily mean (mm), standard deviation (mm) and skew coefficients were also computed for each of the intra-storm stations, and the cosine coefficients were stored in the intra-storm output file.

Storm duration is an important parameter in determining intra-storm characteristics. Normalized storm durations as a function of normalized precipitation depths for the months of May, July and September are shown in Figure 3.5 for Spring Valley, Minnesota. Storm durations were normalized by 24 h, and precipitation depths were normalized by the mean daily precipitation. This figure suggests a weak relationship between storm duration and depth. The parameters and statistics for three different relationships of storm duration with respect to storm depth were analyzed: (1) no trend where the mean and standard deviation were used to summarize the characteristics, (2) linear relationship where the slope of the least square line was computed as well as the mean and standard deviation of residuals, and (3) a logistic relationship. The logistic relationship is described in greater detail below. The best least square fit of the linear and logistic relationships are also shown in Figure 3.5.

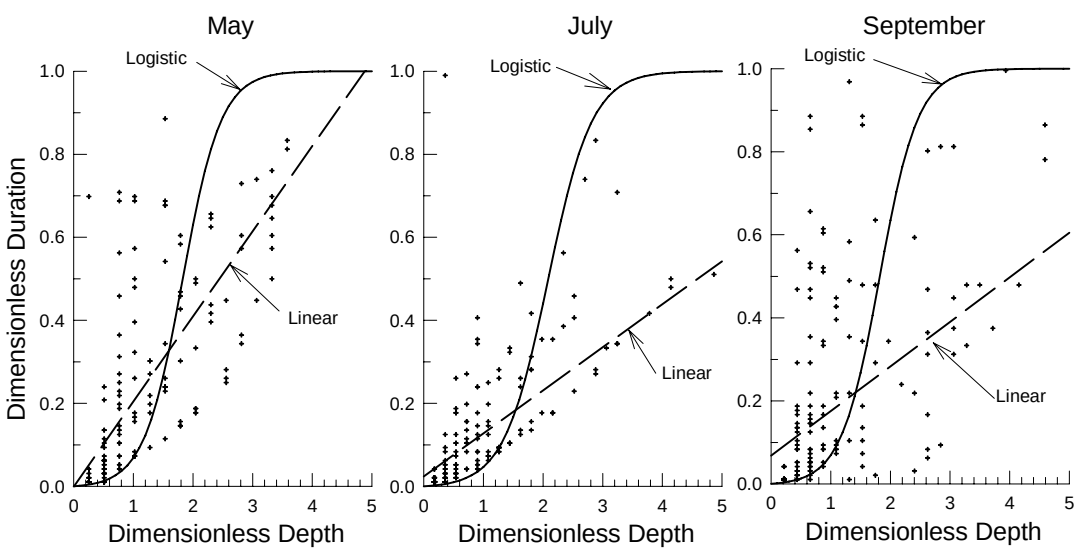


Figure 3.5. Storm Duration as a Function of Precipitation Depth for Spring Valley, MN.

The logistic model was selected to ensure that storm duration is between zero and twenty-four hours. It can be developed by assuming that the relative rate of change in storm duration with depth is directly related to the remaining available time in a day. Let y represent storm duration and x total storm depth. The logistic model can then be represented as

$$\left(\frac{1}{y+\beta}\right)\frac{dy}{dx} = \kappa_1 \left( y_{max} - y \right) \tag{3.7}$$

where dy/dx is the rate of change in storm duration with respect to storm depth, $\kappa_1$ is a rate coefficients, $y_{max}$ is the maximum possible storm duration (i.e., 24 h), and $\beta$ is a base constant. A dimensionless formulation is possible using the variables of $y^*=y/y_{max}$ and $x^*=x/\bar{x}$ ($\bar{x}$ is the mean storm depth). The dimensionless logistic model can then be written as

$$(\frac{1}{y^*+\beta^*})(\frac{1}{1-y^*})\, d\, y^* = \kappa_1\, d\, x^* \tag{3.8}$$

where the additional dimensionless variables are defined as $\beta^*= \beta/y_{max}$ and $\kappa_1^*=\kappa_1\, y_{max}\, \bar{x}$. An analytical solution is obtained by integrating with partial fractions to obtain

$$y^* = \frac{\beta^*[\exp(\kappa_1^*\, x^*(1+\beta^*))-1]}{1+\beta^*\exp(\kappa_1^*\, x^*(1+\beta^*))} \tag{3.9}$$

For each twenty-eight day interval, optimal values for $\beta^*$ and $\kappa_1^*$ were determined using nonlinear regression techniques. Cosine functions were fitted to the data to represent these two parameters within the year. As shown in Figure 3.5, observed duration varied greatly around the logistic function. This variation was evaluated by defining residuals as

$$e_d^* = x^* - \frac{1}{\kappa^*}(\frac{1}{1+\beta^*})\ln[\frac{y^*+\beta^*}{\beta^*(1-y^*)}] \tag{3.10}$$

that is, the residual is defined as the difference in depth and the equivalent predicted depth for a given storm duration. The above formulation allows the prediction of storm duration to be bounded by zero and twenty-four hours. The mean and standard deviation of $e_d$* was computed for each twenty-eight day interval, fitted with cosine functions, and coefficients stored in the intra-storm output file.

Another important intra-storm characteristic is the fraction of the total duration with no precipitation. This fraction is called the no-precipitation gap. The fraction of time with no precipitation is shown in Figure 3.6 for the months of May, July, and September for Spring Valley, Minnesota. Trends in fraction of gap (represented by the symbol g) were evaluated using an exponential function, that is, the rate of change in no-rain gap with storm duration is directly proportional to the remaining available gap fraction, or mathematically,

$$\frac{d\, g}{d\, y} = \kappa(\, g_{max} - g\,) \tag{3.11}$$

where dg/dy is the rate of change in gap fraction with respect to storm duration, κ has units of [1/L], and $g_{max}$ is the maximum gap fraction (i.e., $g_{max}$=1). A dimensionless formulation is obtained using $g^*=g/g_{max}=g$ and $y^*=y/y_{max}$, where $y_{max}$ = 24 h. The above equation can then be written as

$$(\frac{1}{1-g})\,d\,g = \kappa^*\,dy^* \tag{3.12}$$

where $\kappa^*=\kappa/y_{max}$. The above equation can be easily solved for g as

$$g = 1 - \exp(-\kappa^*\,x^*) \tag{3.13}$$

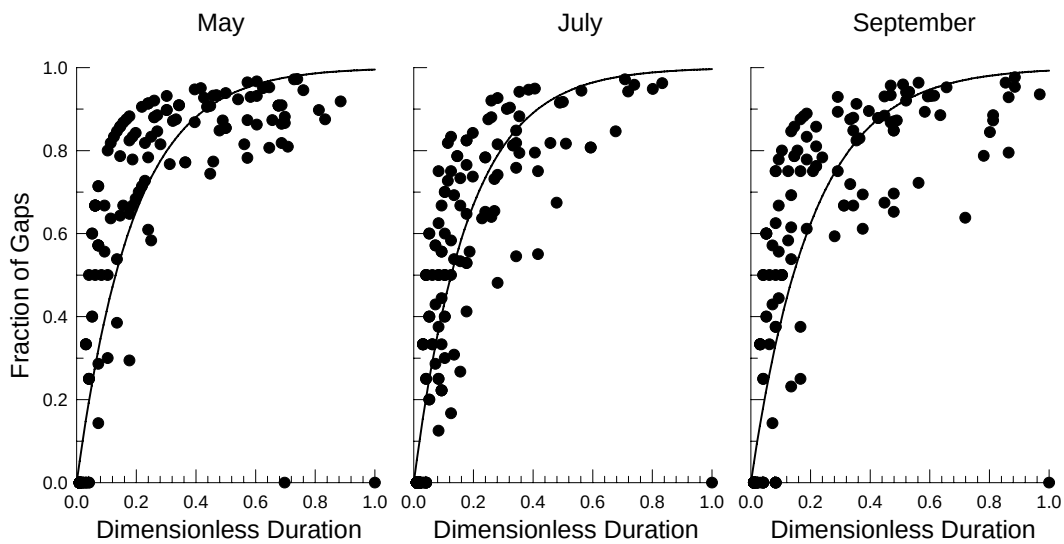


Figure 3.6. Fraction of Time with No Precipitation for Storms At Spring Valley, MN.

The least square estimate of $\kappa^*$ was obtained for each twenty-eight day period using simple log transformation. Trends within the years were captured using the cosine function. An analysis of residuals was done, where residuals were defined as

$$e_g^* = y^* - (-\frac{\ln(1-g)}{\kappa^*}) \tag{3.14}$$

where the twenty-eight day interval's mean and standard deviation are computed from the data set and within-year trends represented by cosine function. To provide the user of the WINDS model with additional options, the mean and standard deviation of fraction of gaps

and the least square slope of a linear relationship and corresponding standard error were also computed and summarized in the output file with coefficients for the cosine curves.

The transitional probabilities ***within*** a storm of wet-wet burst and a wet-dry burst sequences were also computed. The fraction of the storms that had the peak precipitation intensities in the first and fourth quartiles of the storm was determined. For storms with only two rainfall bursts, the fraction of the total precipitation depth in the first burst was also analyzed. All of these statistics were fitted with cosine functions for capturing within-year trends and the coefficients were stored in the precipitation output data file.

The intra-storm characteristics were used to perform a depth-duration-frequency (DDF) analysis. Precipitation depths for return periods of 2 year, 5 year, 10 year, 25 year, 50 year and 100 year for durations of 15 min, 30 min, 45 min, 60 min, 90 min, 2 h, 3 h, 4 h, 6 h, 12 h, and 24 h were computed by first determining the largest depth for each of the duration for each year in the observed data set. The maximum annual time series was converted into a partial duration series by multiplying the annual series values by adjustment factors of 1.13, 1.04, and 1.01 for the 2-y, 5-y, and 10-y depths (Hershfield, 1961). Adjustments were also made to account for differences between clock-time (actual storm duration) and precipitation gathered over a fixed 24 hour period. The following equation was used to adjust to clock time

$$F_d(T) = 2 - \exp[-0.1393(\frac{T}{24})] \tag{3.15}$$

where $F_d(T)$ is the adjustment in depth for a given duration of T (h). For T=24 h, the adjustment corresponds to the recommended value by Hershfield (1961) of 1.13 for daily depths. For D=15 min, the change in precipitation depth is small.

For some intra-storm stations, there were only a few measured storms within a year because of problems with missing data. Determination of the largest precipitation depth is unreliable if only a few of the storms for that year were actually measured. Data for a given year were generally not included if the number of storms was less than 30% of the average number of wet days of a nearby climate station. Exceptions were allowed if one of the storms was a

particularly large event. A large event was defined if the total depth was greater than 10% of the annual precipitation depth, as estimated by a nearby climate station.

The relatively short record length of the intra-storm characteristics made the DDF analysis more difficult. Four different approaches were used to estimate the depths for different return periods and durations. The most straightforward approach relied on the depths obtained mostly from the extreme value type I distribution. For each duration, the plotting position method was used to estimate the depth corresponding to the two-year return period and the extreme value type I distribution was used to estimate the 100-year depth from the mean and standard deviation of the maximum annual time series. Depths corresponding to the 5-y, 10-y, 25-y, and 50-y return periods were determined by interpolating between these two depths using the relationships derived from the extreme value type I (EV1) distribution. Adjustment for conversion to a partial duration series was then done using factors previously described. For some stations, standard deviations of depth for given duration were inconsistent, resulting in unlikely trends in return period depths. The inconsistent standard deviation values were likely caused by insufficient data record length.

The other three approaches used the results of the frequency analysis for a nearby climate station with (usually) a much longer record of daily depths. The "TP-40" approach used the 24-h depth ($P_{F,24}$) obtained from the generalized extreme value (GEV) distribution. The 1-h depth ($P_{F,1}$) was then estimated using the NRCS relationship of $P_{F,1} = 0.46\ P_{F,24}$ for their Type II region (Kent, 1973). For durations between 1 h and 24 h, the relationships embedded in the USWB TP 40 were used (Hershfield, 1961), that is,

$$P_T = P_1 + f_{TP40}\ (P_{24} - P_1) \tag{3.16}$$

where $f_{TP40}$ equaled 0.056, 0.11, 0.22, 0.31, 0.50, and 0.75 for durations of 90 min, 2 h, 3 h, 4 h, 6 h, and 12 h,, respectively. For duration less than 1 h, the 30-minute depth ($P_{F,0.5}$) is estimated using the NRCS relationship of $P_{F,0.5} = 0.37\ P_{F,24}$ for a Type II region. The 15 min depth ($P_{F,0.25}$) and 45-min depth ($P_{F,0.75}$) were computed using relationships embedded in HYDRO-35 (Frederick et al., 1977). These depths were defined as

$$P_{F,0.25} = \frac{P_{F,0.5} - 0.49 P_{F,1}}{0.51} \tag{3.17a}$$

$$P_{F,0.75} = P_{F,0.25} + 0.70\ (P_{F,1} - P_{F,0.25}) \tag{3.17b}$$

The third approach (Weighed Method) for determining the depths for each duration and return period is to combine the results for the EV1 method and the TP-40 method. The depth for the Weighed method is determined by the following equation

$$P_{F,T} = w_1 EV1_{F,T} + w_2 TP40_{F,T} = (\frac{n}{30+n})\ EV1_{F,T} + (\frac{30}{30+n}) TP40_{F,T} \tag{3.18}$$

where n is the number of years used in the estimate of depths using the EV1 method. With this equation, equal weight is given to the EV1 and the TP40 depths for n=30.

The fourth approach used the generalized extreme value (GEV) distribution. Here normalized spread and asymmetric statistics at the nearby long-record climate station were used to estimate the GEV spread and GEV asymmetric statistics for different durations at the intra-storm station. The frequency analysis for the climate station corresponds to the 24-h duration. For the climate station, the GEV spread statistic was normalized by its corresponding mean, and the GEV asymmetric statistic was normalized by its corresponding spread statistic. These normalized statistics were assumed to be constant for all durations of the intra-storm data set. This data set was then only used to compute the mean for each duration from its maximum annual time series. The corresponding intra-storm GEV spread was then obtained by the product of the observed mean and the normalized spread. Likewise, the corresponding intra-storm GEV asymmetric statistic was obtained as the product of the GEV spread and the normalizing asymmetric statistic. Precipitation depths for all of the return periods were then estimated using the GEV distribution from these derived parameters.

The DDF values were summarized by fitting the following breakpoint relationship

$$P_{F,T} = b_0\ F^{b_1}\ T^{b_2}\ (\frac{T_b}{T})^{b_3 \xi} \tag{3.19}$$

where $P_{F,T}$ is the precipitation depth for storm duration T (h) and return period frequency F (y), $T_b$ is the breakpoint duration (set at 1 h), $\xi$ is an indictor variable equal to zero for $T < T_b$ and one for $T > T_b$ and $b_o$, $b_1$, $b_2$, and $b_3$ are coefficients to the DDF values described in the previous paragraphs. The above formulation allows the relationship between depth and

duration to vary to the power of $b_2$ for $T < T_b$ and the power of $b_2$-$b_3$ for $T>T_b$. This provides greater flexibility in fitting Equation 3.19 to the observed data set.

Two different methods were used to estimate the coefficients of $b_o$, $b_1$, $b_2$, and $b_3$. The log-form of Equation 3.19 results in a linear relationship from which the coefficients can be defined easily using the least square estimators. Nonlinear regression analysis was also used. This approach does not require a log-transformation of the data. The fit of Equation 3.19 using the nonlinear regression coefficients is shown in Figure 3.7. The user of the WINDS model has the options of selecting the coefficients obtained by linear or the nonlinear regression methods for DDF values estimated by the EV1 method, the TP40 method, the Weight method, or the GEV method. There are a total of twelve choices. Values are stored in the data file by using a line of output for parameters corresponding to duration less than breakpoint duration (i.e., $\xi = 0$). Here the log-intercept parameter, $b_o$, the power of frequency, $b_1$, and power of duration, $b_2$, are stored. Another line of output is used for the parameters corresponding to duration greater than the breakpoint duration (i.e., $\xi = 1$). The log-intercept parameter, $b_o T_b^{b3}$, the power of frequency, $b_1$, and power of duration, $(b_2 - b_3)$, are stored in the data file.

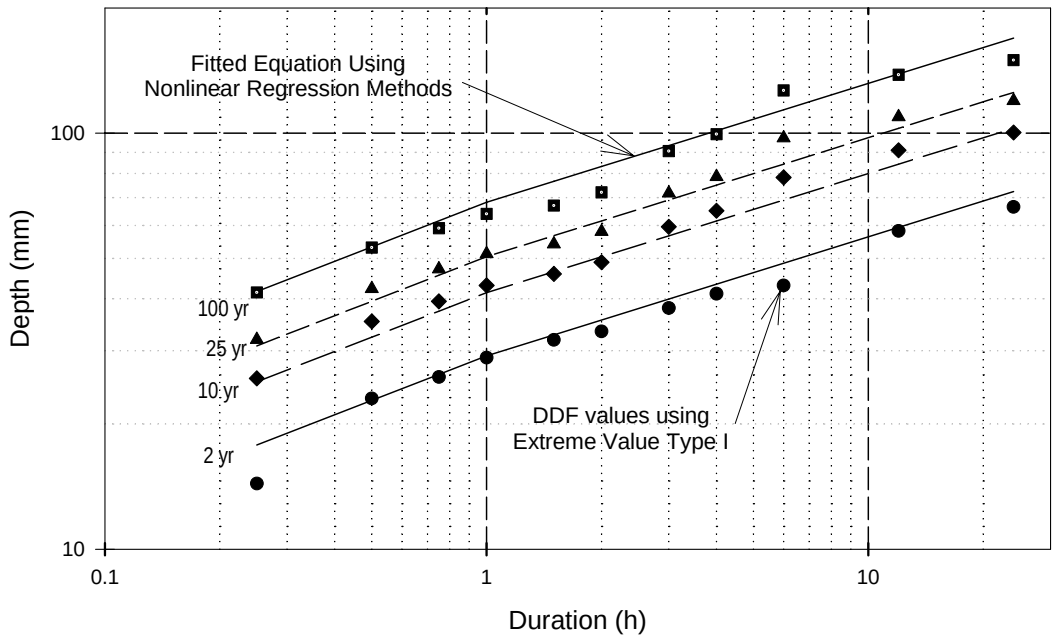


Figure 3.7. DDF values and Fitted Function for Holyoke, MN

The DDF values obtained at the intra-storm stations were converted to normalized values for a nearby daily climate station by using the following equation

$$P^*_{F,T} = \left(\frac{P^c_{F,24h}}{P_{F,24h}}\right)\left(\frac{P_T}{P^c_{2y,24h}}\right) \tag{3.30}$$

where $P^*_{F,T}$ is the normalized depth for a given return period (F) and duration (T). All depths were normalized by the 2-y, 24-h depth available at the climate station (superscript c). Depths were also adjusted by the ratio of F-y, 24-h depth at the climate station to that at the intra-storm station. The DDF curve used to summarize the normalized DDF value can be written as

$$P^*_{F,T} = \frac{P_{F,T}}{P_{2y,24h}} = \frac{b_0\ F^{b_1}\ T^{b_2}\ \left(\frac{T_b/24}{T/24}\right)^{b_3\xi}}{b_0\ (2)^{b_1}\ (24)^{b_2}\ \left(\frac{T_b}{24}\right)^{b_3}} = b^*_o\ F^{*b_1}\ T^{*b_2}\ \left(\frac{T^*_b}{T^*}\right)^{b_3\xi} \tag{3.21}$$

where $F^* = F/2$, $T^* = T/24$, $T_b^* = T_b/24$ and $b_o^* = (T_b^*)^{-b3}$. Since the DDF values are not represented perfectly by the DDF curve, linear and nonlinear regression methods were applied to Equation 3.21 to determine the coefficients $b_o^*$, $b_1$, $b_2$, and $b_3$ for each of the four different methods for computing $P_{F,T}$. The eight sets of coefficients are stored in the output file for daily climate variables as well the normalizing 2-y depth. Coefficients are stored as

the log-intercept, power of frequency, and power of duration in separate lines for duration less than and greater than the breakpoint duration.

## Prediction of Daily Climate Variables

*Introduction*

Prediction of daily climate variables is done by selecting statistical methods to simulate a time series of values that have similar statistical characteristics to those observed. Let's consider a hypothetical time series plot of daily temperature and rainfall intensity as shown in Figure 3.8. In this figure, temperature appears to be well represented as a continuous curve. Continuous variables are usually simulated within a statistical framework as Markov processes. The rainfall intensity in Figure 3.8 appears to be discontinuous as the rainfall intensity sudden jumps from zero to a non-zero value because of a sudden burst of precipitation. A sequence of precipitation events may then be best represented as discrete events of wet and dry days. The simulation of discrete events within a statistical framework is usually done using Markov chains. Here the probability of a transition from a dry to a wet day or from a wet to a dry day is of fundamental importance. After a day has been determined to be wet, the total depth can be estimated from a specified probability density function with appropriate statistical parameters.

A summary of daily weather variables predicted by the WINDS model is given in Table 3.1 Non-precipitation variables are simulated as Markov processes. Daily precipitation depth is predicted using a Markov chain for discrete dry-and-wet day events that is coupled with a depth estimate from a specified probability density function. Details of these methods are given in three sections. The first section describes methods used in WINDS for predicting uncorrelated non-precipitation weather variables. This is the simplest option and is the most robust approach. The second section describes methods used to predict non-precipitation variables such that cross-correlations among key weather variables are maintained. The final section discusses the approach used to compute daily precipitation depth.

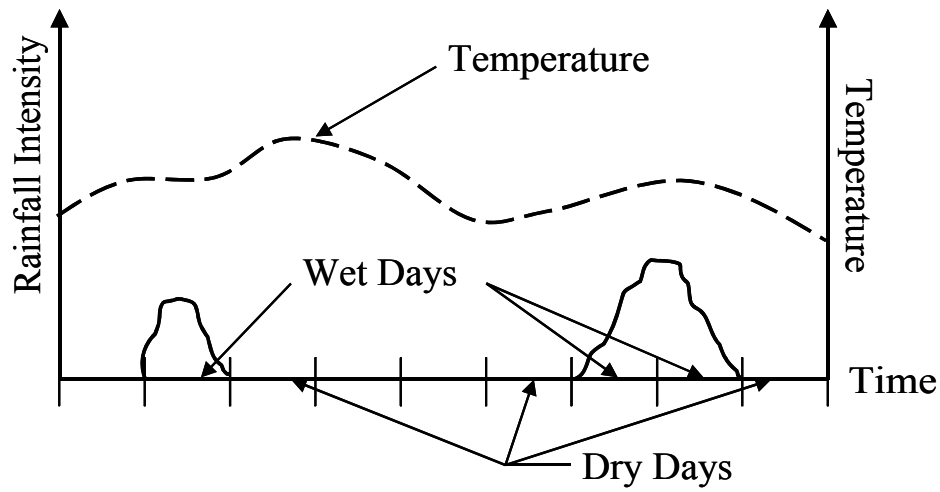


Figure 3.8.Hypothetical Time Series of Temperature and Rainfall Intensity.

The prediction of daily weather variables is fundamentally related to random processes or events. It is therefore possible, especially for the uncorrelated weather option, that for any particular day that the predicted minimum temperature is greater than the predicted maximum, that the predicted minimum relative humidity is greater than the predicted maximum, that the predicted maximum wind speed is less than the predicted average, and that the predicted dew point temperature is greater than the predicted maximum temperature. Appropriate checks are placed in the code to prevent these inconsistencies.

*Uncorrelated Non-Precipitation Weather Variables*

The simplest and most robust option for the user is to select uncorrelated non-precipitation weather variables. For this option, weather variables are predicted independently of each other. For example, minimum temperature is not influenced by the maximum temperature for that day. However, serial correlation with the previous day is included in the simulation approach. In the WINDS model, non-precipitation variables are predicted using a first-order autoregressive model. This model is defined as

$$X_t = \mu_x + \rho_{x1}(X_{t-1} - \mu_x) + \varepsilon_t \tag{3.22}$$

where $X_t$ is the predicted value (e.g., maximum temperature for day t), $X_{t-1}$ is the predicted value of the previous day, $\mu_x$ is the mean value, and $\varepsilon_t$ is a random error.

As discussed in the previous section, the standard deviation and the skew coefficient for all of the weather variables were computed, and appropriate cosine coefficient stored into an input file for the WINDS model. The standard deviation and the coefficient of variation of the error term in Equation 3.22 can be related to the standard deviation and the skew coefficient of the weather variable using

$$\sigma_{\varepsilon} = \sigma_x \sqrt{1-\rho_1^2} \tag{3.23a}$$

$$C_{s\varepsilon} = C_{sx} \left( \frac{1-\rho_1^3}{(1-\rho_1^2)^{3/2}} \right) \tag{3.23b}$$

The key parameters of Equation 3.22 can be obtained from the information stored in the daily climate file. The mean and standard deviation are obtained as

$$STAT(X_t) = X_{std}\,[b_o + b_1 \cos(t_t + b_2) + b_3 \cos(2t_t + b_4) + b_5 \cos(3t_t + b_6)\,] \tag{3.24}$$

where $STAT(X_t)$ is the mean and the standard deviation of the weather variable of interest, where $t_t = 2t\pi/365$ and $X_{std}$ is the normalizing value (also stored in the daily climate file). The serial correlation coefficient and the skew coefficient are defined using a form of Equation 3.24 for $X_{std} = 1$. The user has the choice of selecting a random error using the normal distribution or the extreme value type I distribution. Both use a mean of zero. The normal distribution should be selected for most applications.

Means, standard deviations, and skew coefficients may differ between days with and without precipitation. Since these statistics were computed for all days (wet and dry), only dry days, and only wet days, the user can select to vary means, standard deviations, and skew coefficients depending on the precipitation state of the day.

*Correlated Non-Precipitation Variables*

The procedures outlined by Matalas (1967) are used to simulate cross-correlations and additional serial correlations between key weather variables. This approach requires the solution of the following system of equations, corresponding to j=1 to n weather variables,

$$\mathbf{x}_t = \mathbf{A}\,\mathbf{x}_{t-1} + \mathbf{B}\,\boldsymbol{\varepsilon}_t \tag{3.25}$$

where **A** and **B** are nxn matrices, $\mathbf{x}_t$, $\mathbf{x}_{t-1}$ and $\boldsymbol{\varepsilon}_t$ are vectors (nx1) corresponding to day t and the previous day t-1. The jth elements of the $\mathbf{x}_{t-1}$ and the $\mathbf{x}_t$ vectors are defined as

$$x_{t\text{-}1,j} = X_{t\text{-}1,j} - \mu_{t-1,j} \text{ and } x_{t,j} = X_{t,j} - \mu_{t,j} \tag{3.26}$$

For conditions of no correlation between the error term and the weather variables and for errors with a mean of zero and a standard deviation of one, correlations can be maintained if the matrix **A** of Equation 3.25 is defined as

$$\mathbf{A} = \mathbf{M}_1 \, \mathbf{M}_0^{-1} \tag{3.27a}$$

and the matrix **B** is defined as

$$\mathbf{B}\mathbf{B}^T = \mathbf{M}_0 - \mathbf{M}_1 \, \mathbf{M}_0^{-1} \, \mathbf{M}_1^T \tag{3.27b}$$

where $\mathbf{M}_o$ is the symmetrical cross-covariance matrix defined as

$$\mathbf{M}_0 = \begin{bmatrix} VAR(x_{t-1,1}) & \dots & COV(x_{t-1,1}, x_{t-1,n}) \\ \vdots & \ddots & \vdots \\ COV(x_{t-1,n}, x_{t-1,1}) & \dots & VAR(x_{t-1,n}) \end{bmatrix} \tag{3.28a}$$

and $\mathbf{M}_1$ is the asymmetrical serial covariance matrix defined as

$$\mathbf{M}_1 = \begin{bmatrix} COV(x_{t,1}, x_{t-1,1}) & \dots & COV(x_{t,1}, x_{t-1,n}) \\ \vdots & \ddots & \vdots \\ COV(x_{t,n}, x_{t-1,1}) & \dots & COV(x_{t,n}, x_{t-1,n}) \end{bmatrix} \tag{3.28b}$$

The solution to matrix **A** is obtained using standard algorithms for working with matrices. The solution to matrix **B** is obtained using the classic eigenvalue formulation defined for the above matrices as

$$(\mathbf{B}\,\mathbf{B}^{\mathbf{T}} - \lambda_1 \mathbf{I})\,\mathbf{u}_1 = \mathbf{0} \tag{3.29}$$

where $\mathbf{B}\mathbf{B}^{\mathbf{T}}$ is a nxn matrix, $\lambda_1$ is a scalar value called the eigenvalue and $\mathbf{u}_1$ is the eigenvector. There are n solutions for $\lambda_i$ and corresponding $\mathbf{u}_i$. Eigenvectors will also be subject to the normalizing constraint that $\mathbf{u}_i^T\mathbf{u}_i = 1$.

The eigenvalue formulation can be manipulated as

$$\mathbf{u}_i^T\,(\mathbf{B}\,\mathbf{B}^{\mathbf{T}} - \lambda_i\,\mathbf{I})\,\mathbf{u}_i = \mathbf{u}_i^T\mathbf{B}\,\mathbf{B}^{\mathbf{T}}\mathbf{u}_i - \lambda_i\,\mathbf{u}_i^T\,\mathbf{u}_i = \mathbf{u}_i^T\mathbf{B}\,\mathbf{B}^{\mathbf{T}}\mathbf{u}_i - \lambda_i = \mathbf{0} \tag{3.30a}$$

where $\mathbf{u}_i^T\mathbf{u}_i = 1$ has been used. We conclude

$$\mathbf{u}_i^T\mathbf{B}\,\mathbf{B}^{\mathbf{T}}\mathbf{u}_i = \lambda_i \tag{3.30b}$$

By repeating this process for all eigenvectors, we have the following set of equations

$$\mathbf{U}^{\mathbf{T}}\mathbf{B}\,\mathbf{B}^{\mathbf{T}}\mathbf{U} = \begin{bmatrix} \lambda_1 & \dots & 0 \\ \vdots & \ddots & \vdots \\ 0 & \dots & \lambda_n \end{bmatrix} = \begin{bmatrix} \sqrt{\lambda_1} & \dots & 0 \\ \vdots & \ddots & \vdots \\ 0 & \dots & \sqrt{\lambda_n} \end{bmatrix} \begin{bmatrix} \sqrt{\lambda_1} & \dots & 0 \\ \vdots & \ddots & \vdots \\ 0 & \dots & \sqrt{\lambda_n} \end{bmatrix} = \mathbf{D}\,\mathbf{D} \tag{3.31}$$

where **U** is the matrix where the columns corresponding to each set of eigenvectors and **D** is a diagonal matrix where the elements are the square root of eigenvalues. This requires that all **eigenvalues are positive**.

By using matrix multiplication rules, we obtain

$$\mathbf{U}^{\mathbf{T}}\mathbf{B}\,\mathbf{B}^{\mathbf{T}}\mathbf{U}\mathbf{U}^{-1} = \mathbf{U}^{\mathbf{T}}\mathbf{B}\,\mathbf{B}^{\mathbf{T}} = \mathbf{D}\,\mathbf{D}\mathbf{U}^{-1} \tag{3.32a}$$

and with additional multiplication

$$(\mathbf{U}^{\mathbf{T}})^{-1}\mathbf{U}^{\mathbf{T}}\mathbf{B}\,\mathbf{B}^{\mathbf{T}} = \mathbf{B}\,\mathbf{B}^{\mathbf{T}} = (\mathbf{U}^{\mathbf{T}})^{-1}\mathbf{D}\,\mathbf{D}\mathbf{U}^{-1} = (\mathbf{U}^{-1})^{T}\,\mathbf{D}\,\mathbf{D}\mathbf{U}^{-1} \tag{3.32b}$$

where the matrix rule of $(\mathbf{U}^{\mathbf{T}})^{-1} = (\mathbf{U}^{-1})^{\mathbf{T}}$ has been used. Let's define **B** as

$$\mathbf{B} = (\mathbf{U}^{-1})^{T}\,\mathbf{D} \tag{3.33}$$

By using the matrix rule that $(\mathbf{E}\,\mathbf{F})^{\mathbf{T}} = \mathbf{E}^{\mathbf{T}}\,\mathbf{F}^{\mathbf{T}}$, we then obtain

$$\mathbf{B}^{T} = \mathbf{D}\,\mathbf{U}^{-1} \tag{3.34}$$

and the conditions of Equation 3.32b are satisfied.

In the WINDS model, the matrices **A** and **B** of Equation 3.25 are constant for five-day intervals. For each of the five-day intervals, the elements of matrices $\mathbf{M}_o$ and $\mathbf{M}_1$ are defined by using the cosine function of the form of Equation 3.24. As previously discussed, the appropriate cosine coefficients have been stored for cross correlation and serial correlation coefficients. The $X_{std}$ in Equation 3.24 is replaced by the product of appropriate standard deviations. The midpoint of the five-day interval is used in the cosine function. The algorithm used to compute eigenvectors requires a symmetrical matrix for $\mathbf{M}_1$**.** The upper diagonal elements of this matrix are used to define the lower diagonal elements. The matrix **A** is computed using well-established algorithms to solve Equation 3.27a for each five-day interval within the year.

The matrix **B** is obtained by Equation 3.33. The determination of the eigenvectors for the **U**

matrix and eigenvalues for the **D** matrix is an important step in this computation. Initial attempts to maintain correlations among all weather variables resulted in negative eigenvalues, preventing a solution. Therefore, the only non-zero off-diagonal elements are those for cross and serial correlations between (1) maximum and minimum temperatures, (2) maximum temperature and radiation, (3) maximum and minimum relative humidity, and (4) dewpoint temperature and minimum relative humidity. If negative eigenvalues still occur with these variables, the correlations are systematically reduced until only positive eigenvalues are obtained. A different set of elements are obtained for matrix **B** for each five-day interval.

Predicted statistical characteristics for maximum temperature and maximum relative humidity are shown in Figures 3.9 and 3.10, respectively. The solid curves in these figures are the cosine curves obtained from observed climate data, and therefore effectively correspond to observed values. The mean and standard deviation of the predicted maximum temperature are in good agreement to the observed trends. The skew coefficient of normally distributed values is zero, and therefore the theoretical structure prevents the prediction of values resulting in a non-zero skew coefficient. The predicted statistics of the maximum relative humidity are not as accurate as those obtained for maximum temperature. This is, at least partially, caused by the WINDS model limiting the maximum relative humidity to 100%.

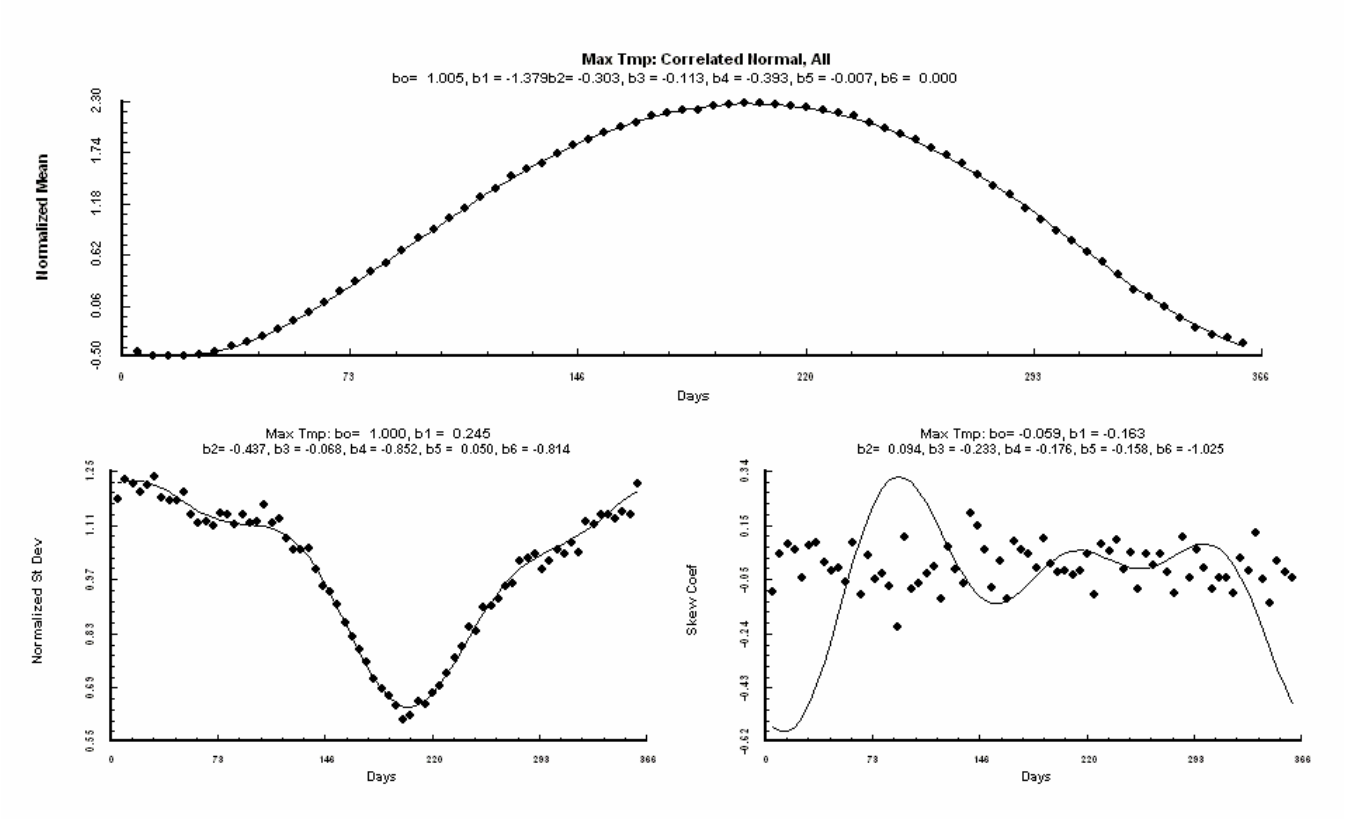


Figure 3.9 Predicted Statistical Characteristics of Maximum Temperature at Rochester, MN.

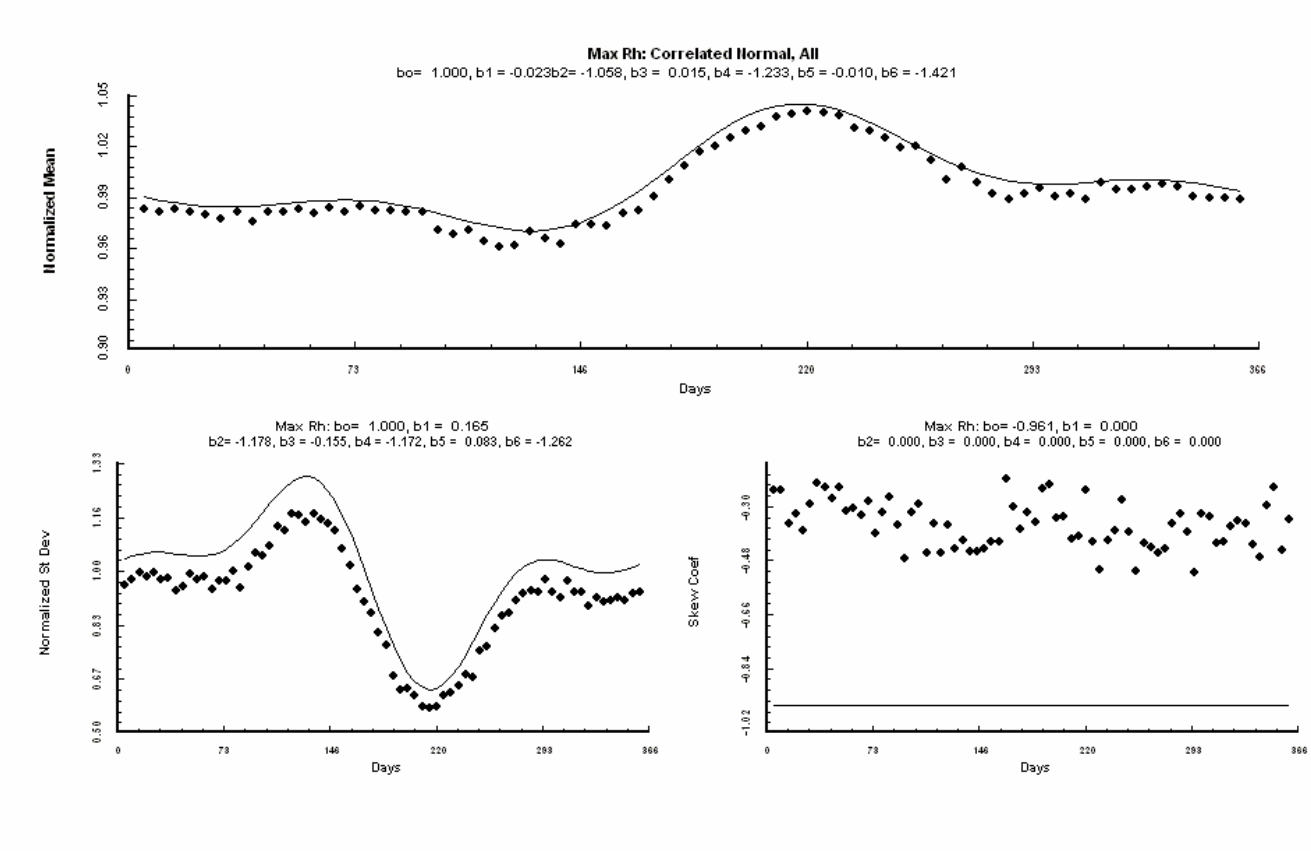


Figure 3.10. Predicted Statistical Characteristics of Maximum Relative Humidity at Rochester, MN.

Predicted cross correlation coefficients among minimum relative humidity and selected weather variables are shown in Figure 3.11, and predicted serial correlation coefficients among dewpoint temperature and selected weather variables are shown in Figure 3.12. The predicted cross and serial correlation coefficients are approximately zero for all variables, except those identified for correlation. The coefficients for these variables are in good agreement to those observed. The dewpoint temperature was selected to be correlated with minimum relative humidity. Since minimum relative humidity is correlated to maximum relative humidity, some serial correlation with maximum relative humidity is still maintained.

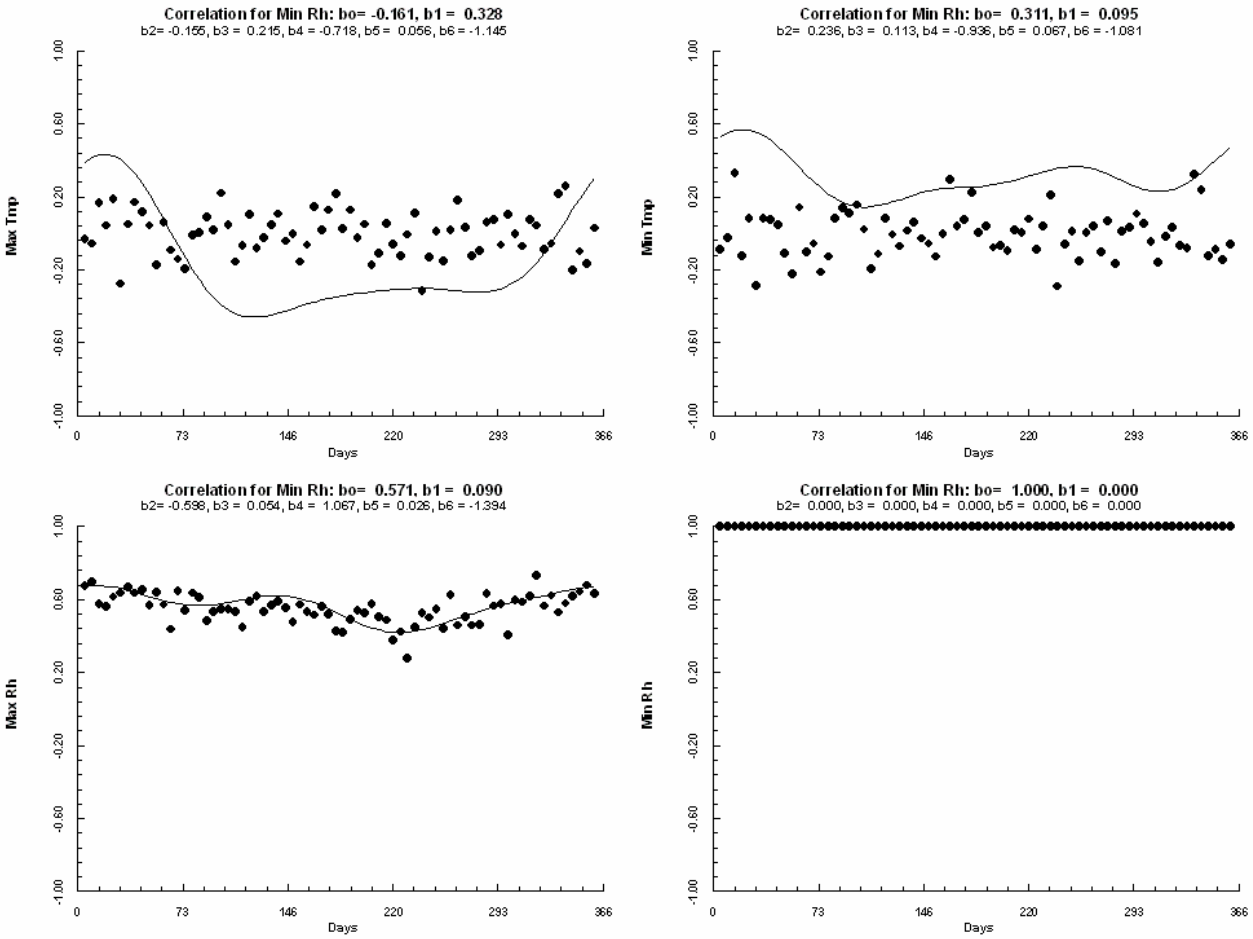


Figure 3.11. Cross Correlation Coefficients between Minimum Relative Humidity and Selected Weather Variables at Rochester, MN.

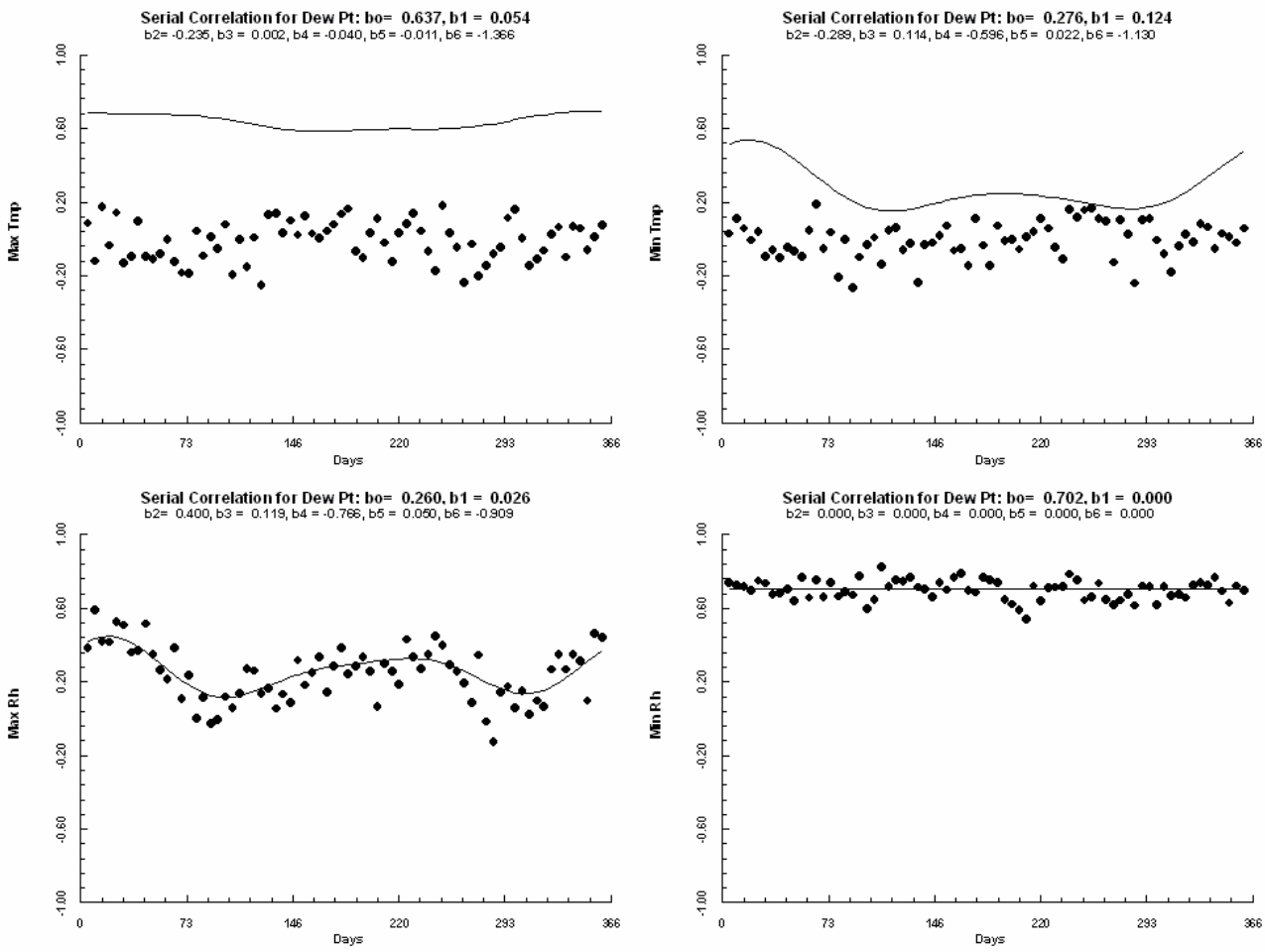


Figure 3.12. Serial Correlation Coefficients between Dewpoint Temperature and Selected Weather Variables at Rochester, MN.

*Simulation of Daily Precipitation*

The simulation of daily precipitation is done by coupling a first-order Markov chain with a probability density function of daily rainfall depth. The first step is the determination of whether the discrete precipitation state is a wet day, where a wet day is simply a day with precipitation. This is done using the transitional probability of wet day given that the previous day is dry or the transitional probability of wet day given that the previous day is a dry day. These transitional probabilities were computed from the daily climate data and are summarized using coefficients of the cosine function stored in the daily climate file. If the

day is not a wet day, then by definition it is a dry day. As previously discussed, the user can use the precipitation state of the day to determine the mean, standard deviation, and skew coefficient of the non-precipitation weather variables.

The storm depth for a wet day is computed from a probability density function. The user can select either an exponential, log-normal, extreme value type I, gamma (skew normal), or generalized extreme value (GEV) distribution. The daily precipitation at the climate station was analyzed to determine the daily mean, standard deviation, skew coefficient, GEV spread statistic, and the GEV asymmetric statistics. The appropriate value for any day can be determined from the coefficients of the cosine function stored in the daily climate file.

The predicted daily precipitation statistics are shown in the observed cosine curves in Figure 3.13 for Rochester, Minnesota. The predicted daily precipitation statistics are in good agreement with observed trends. The predicted and observed annual precipitation depth and average annual number of wet days are shown in Figure 3.14. The WINDS model predicted these statistics with good accuracy.

## Prediction of Storm Characteristics

*Theoretical Framework*

Intra-storm characteristics of the WINDS model are predicted using the general framework proposed by Wilson and Headrick (1998) for a known storm depth and duration. It is based on the theoretical concepts of Keifer and Chu (1957), often referred to as the Chicago hyetograph method. The overall goal of the method is to develop storm patterns that match known depth-duration-frequency values (DDF) for a site. The breakpoint form of the DDF equation was previously given by Equation 3.19. It will be evaluated here in the following form:

$$P = K_i \, F^{b_1} \, T^{n_i} \tag{3.35}$$

where for $T < T_b$, $K_i = K_1 = b_o$ and $n_i = n_1 = b_2$ and for $T > T_b$, $K_i = K_2 = b_o T_b^{b3}$ and $n_i = n_2 = b_2 - b_3$.

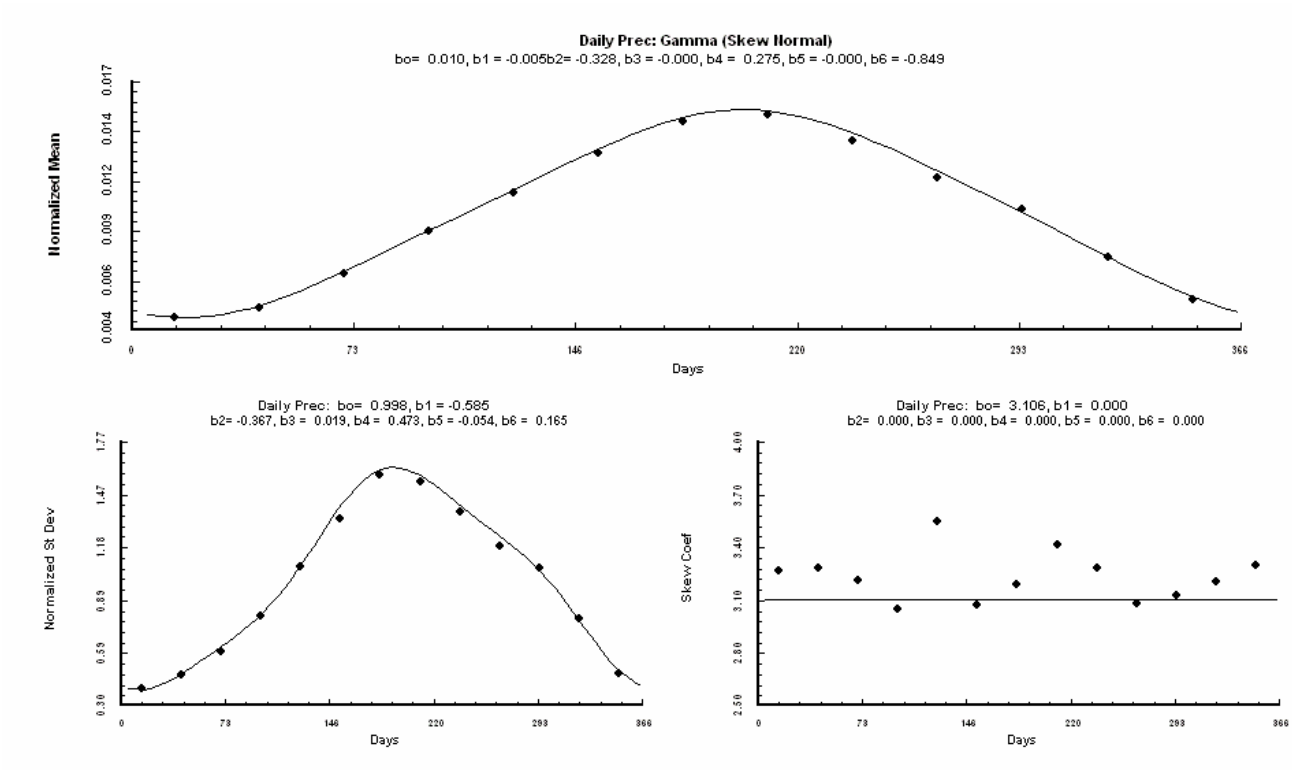


Figure 3.13. Predicted Daily Precipitation Statistics for Rochester, MN.

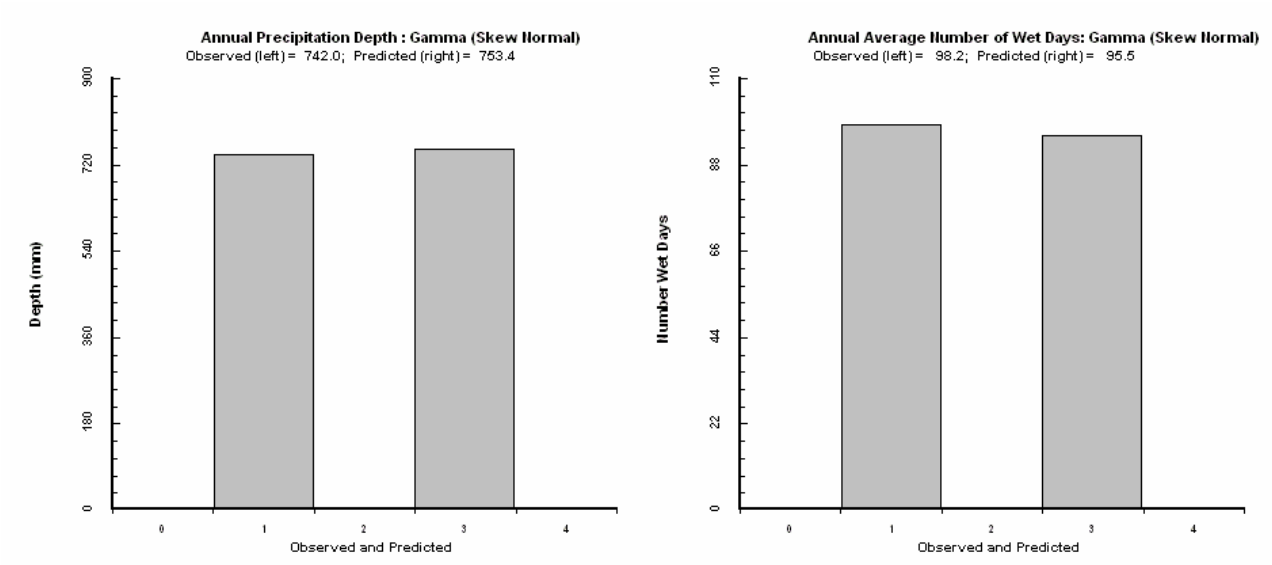


Figure 3.14. Predicted and Observed Annual Precipitation Depth and Number of Wet Days for Rochester, MN.

Total storm depth is known for each wet day by using the algorithms discussed in the

previous section. Later in this section, the methods to compute storm duration are described. The total storm depth ($P_s$) and total storm duration ($T_s$) are therefore known. A key assumption is that cumulative depths for all durations less than the storm duration have the same frequency.

A dimensionless form of Equation 3.19 is obtained by dividing both sides of this equation by $P_s$, corresponding to storm duration of $T_s$. We then obtain

$$P_* = \frac{P_T}{P_s} = \frac{b_0\ F^{b_1}\ T^{b_2}\ (\frac{T_b}{T})^{b_3\xi}}{b_0\ F^{b_1}\ T_s^{b_2}\ (\frac{T_b}{T_s})^{b_3\xi}} = \alpha_*\ T_*^n \tag{3.36}$$

where $P_*$ is the cumulative precipitation normalized by storm depth and $T_*$ is the cumulative time (duration) normalized by storm duration. The symbols $\alpha_*$ and n have the following definitions

$$\alpha_* = 1,\ n = n_1 = b_2 \qquad T < T_b,\quad T_s < T_b \tag{3.37a}$$

$$\alpha_* = \frac{T_s^{b_3}}{T_b^{b_3}} = (\frac{K_1}{K_2}) T_s^{n_1 - n_2},\ n = b_2 \qquad T < T_b,\quad T_s > T_b \tag{3.37b}$$

$$\alpha_* = 1,\ n = n_2 = b_2 - b_3 \qquad T > T_b,\quad T_s > T_b \tag{3.37c}$$

Dimensionless rainfall intensity is directly defined as

$$\mathrm{I}_* = \frac{\mathrm{d\,P_*}}{\mathrm{d\,T_*}} = \alpha_*\ \mathrm{n\ T_*} = \frac{\mathrm{d\,P\,/\,d\,T}}{\mathrm{P_s}\,/\,T_s} \tag{3.38}$$

which is physically defined as the rainfall intensity normalized by the average intensity for the storm.

Equation 3.36 can be used to determine the cumulative depth of precipitation within a storm. This equation assumes that the peak rainfall intensity occurs at the beginning of the storm. A more general solution can be obtained for different times of peak intensity. The solution approaches are shown in Figure 3.15. The left-sided figure corresponds to the solution for peak intensity at $T_*=0$ as given by Equation 3.36. The right-sided figure is the rainfall intensity for a peak intensity at $t_*=t_{*p}$. The endpoints of the right-side pattern are defined to equal the storm duration, that is, $T_* = t_{*R} - t_{*L}$.

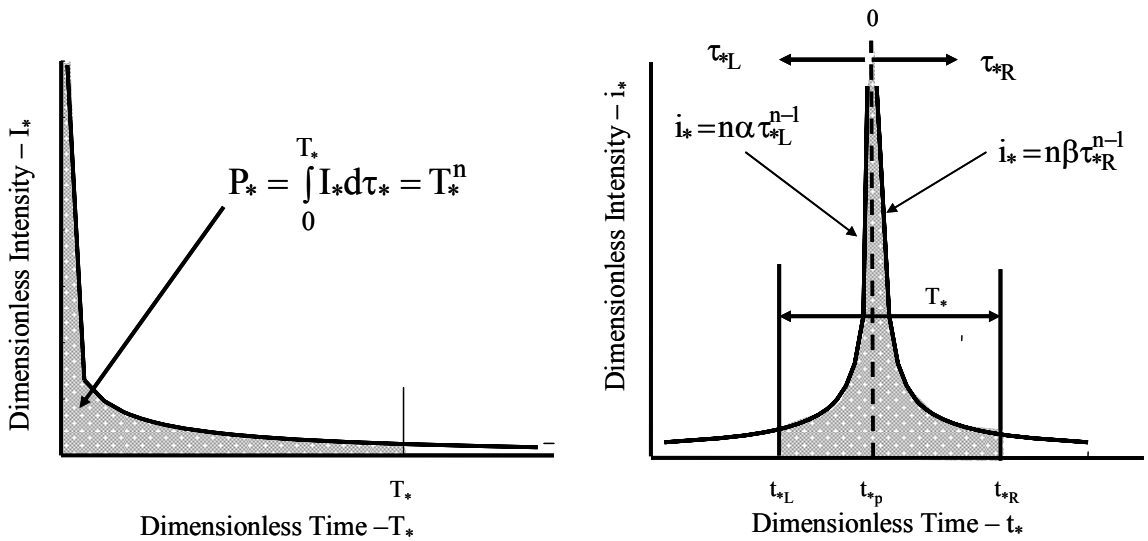


Figure 3.15. Hyetographs Derived from DDF Curves.

The fraction of the duration corresponding to the left (rising) limb ($l_*$) is defined as

$$l_* = \frac{t_{*p} - t_{*L}}{T_*} = t_{*p} \tag{3.39a}$$

where the last equality is obtained using the entire storm duration (i.e., $T_* = 1$ and $t_{*L} = 0$). A constant $l_*$ for durations within a storm is used in deriving the hyetograph. The fraction of the duration corresponding to the right (falling) limb ($r_*$) is defined as

$$r_* = \frac{t_{*R} - t_{*p}}{T_*} = 1 - l_* = 1 - t_{*p} \tag{3.39b}$$

Cumulative precipitation depths are equal for the same duration for the two patterns shown in Figure 3.15. The intra-storm intensities for the right-sided figure are defined as a power function of the form relative to the time of peak intensities. Unknown coefficients A and B are defined such that the partition of precipitation between the rising and falling limbs is done in proportion to $l_*$ and $r_*$ for their respective limb. Let's consider the change in cumulative depth over a small time increment, that is, $\Delta P_* = I_* \Delta T_*$. The partitioning of this precipitation depth between rising and falling limbs can be done using

$$l_* \, I_* \, \Delta T_* = A \alpha_* n \, \tau_L^{n-1} \Delta \tau_L \text{ and } r_* \, I_* \, \Delta T_* = B \alpha_* n \, \tau_R^{n-1} \Delta \tau_R \tag{3.40a}$$

where the first equation corresponds to the rising limb and the second to the falling limb and where $\tau_L = t_{*p} - t_*$ and $\tau_R = t_* - t_{*p}$. By using Equation 3.38, $\Delta\tau_L = l_* \Delta T_*$, and $\Delta\tau_R = r_* \Delta T_*$, we obtain

$$T_*^{n-1} = A\,(t_{*p} - t_*)^{n-1} \quad \text{and} \quad T_*^{n-1} = B\,(t_* - t_{*p})^{n-1} \tag{3.40b}$$

and therefore A and B are defined as

$$A = \frac{T_*^{n-1}}{(t_{*p} - t_*)^{n-1}} = \frac{1}{t_{*p}^{n-1}} \quad \text{and} \quad B = \frac{T_*^{n-1}}{(t_* - t_{*p})^{n-1}} = \frac{1}{(1 - t_{*p})^{n-1}} \tag{3.41}$$

The dimensionless rainfall intensities for the rising and falling limbs can then be written as

$$i_{*L} = \alpha_*\, n\, \left(\frac{t_{*p} - t_*}{t_{*p}}\right)^{n-1} \quad \text{and} \quad i_{*R} = \alpha_*\, n\, \left(\frac{t_* - t_{*p}}{1 - t_{*p}}\right)^{n-1} \tag{3.42}$$

Let's consider the relatively simple hyetograph for $\mathbf{T_s \le T_b}$**.** For this case, $\alpha_* = 1$ and $n = b_2$. By using the intensity defined by Equation 3.42, the cumulative depth for the rising limb of the hyetograph is defined as

$$p_*(\hat{t}_*) = n_1 \int_0^{t_*} \left(\frac{t_{*p} - t_*}{t_{*p}}\right)^{n-1} dt_* = n_1 t_{*p} \int_{\hat{t}_*}^{1} \hat{t}_*^{\,n_1 - 1}\, d\hat{t}_* = t_{*p}(1 - \hat{t}_*^{\,n_1}) \tag{3.43a}$$

$$\textit{for } t_* \le t_{*p},\ T_s \le T_b$$

where

$$\hat{t}_* = \frac{t_{*p} - t_*}{t_{*p}} = 1 - \frac{t_*}{t_{*p}} \tag{3.43b}$$

Likewise, the cumulative depth for the falling limb of the hyetograph is defined as

$$p_*(\tilde{t}_*) = t_{*p} + n_1 \int_{t_{*p}}^{t_*} \left(\frac{t_* - t_{*p}}{1 - t_{*p}}\right)^{n_1 - 1} dt_* = t_{*p} + n_1(1 - t_{*p}) \int_0^{\tilde{t}_*} \tilde{t}_*^{\,n_1 - 1}\, d\tilde{t}_* = \tag{3.44a}$$

$$t_{*p} + (1 - t_{*p})\tilde{t}_*^{\,n_1} \quad \textit{for } t_* > t_{*p},\ T_s \le T_b$$

where

$$\tilde{t}_* = \frac{t_* - t_{*p}}{1 - t_{*p}} \tag{3.44b}$$

Let's now consider the hyetograph for $\mathbf{T_s > T_b}$**.** In addition to determining separate relationships for the rising and falling limbs, relationships are needed to account for each of the piecewise DDF curves. By using the definitions for l* and r*, these durations are defined as

$$t_{*Lb} = t_{*p} - l_* T_{*b} = t_{*p}(1 - T_{*b}) \text{ and } t_{*Rb} = t_{*p} + (1 - t_{*p}) T_{*b} \tag{3.45}$$

By using the intensities given by Equation 3.42, the cumulative depth for the ***rising limb*** and for $\boldsymbol{0 \le t_* \le t_{*Lb}}$ can be defined as

$$p_*(\hat{t}_*) = n_2 \int_0^{t_*} \left(\frac{t_{*p} - t_*}{t_{*p}}\right)^{n_2 - 1} dt_* = n_2 t_{*p} \int_{\hat{t}_*}^{1} \hat{t}_*^{n_2 - 1}\, d\hat{t}_* = t_{*p}(1 - \hat{t}_*^{n_2}) \tag{3.46a}$$

$$for\ 0 \le t_* \le t_{*Lb},\ T_s > T_b$$

and for $\boldsymbol{t_{*Lb} \le t_* \le t_{*p}}$ can be defined as

$$p_*(\hat{t}_*) = t_{*p}(1 - \hat{t}_{*Lb}^{n2}) + n_1 \alpha_* \int_{t_{*Lb}}^{t_*} \left(\frac{t_{*p} - t_*}{t_{*p}}\right)^{n_1 - 1} dt_* = t_{*p}(1 - \hat{t}_{*Lb}^{n2}) + n_1 \alpha_* t_{*p} \int_{\hat{t}_*}^{\hat{t}_{*Lb}} \hat{t}_*^{n_1 - 1}\, d\hat{t}_* = \tag{3.46b}$$

$$t_{*p}(1 - \hat{t}_{*Lb}^{n_2} + \alpha_* \hat{t}_{*Lb}^{n_1} - \alpha_* \hat{t}_*^{n_1}) \quad for\ t_{*Lb} \le t_* \le t_{*p},\ T_s > T_b$$

where $\hat{t}_*$ is as previously defined.

By using the intensities given by Equations 3.42, the cumulative depth for the **falling limb** and for $\mathbf{t_{*Rb} \le t_* \le 1}$

$$p_*(\tilde{t}_*) = p_*(t_{*p}) + n_1 \alpha_* \int_{t_{*p}}^{t_*} \left(\frac{t_* - t_{*p}}{1 - t_{*p}}\right)^{n_1 - 1} dt_* = p_*(t_{*p}) + n_1 \alpha_* (1 - t_{*p}) \int_0^{\tilde{t}_*} \tilde{t}_*^{n_1 - 1}\, d\tilde{t}_* = \tag{3.47a}$$

$$t_{*p}(1 - \tilde{t}_{*Lb}^{n_2} + \alpha_* \tilde{t}_{*Lb}^{n_1}) + \alpha_*(1 - t_{*p}) \tilde{t}_*^{n_1} \quad for\ t_{*p} \le t_* \le t_{*Rb},\ T_s > T_b$$

and for $\mathbf{t_{*p} \le t_* \le t_{*Rb}}$

$$p_*(\tilde{t}_*) = p_*(t_{*p}) + n_2 \int_{t_{*Rb}}^{t_*} \left(\frac{t_* - t_{*p}}{1 - t_{*p}}\right)^{n_1 - 1} dt_* = p_*(t_{*p}) + n_2 \alpha_* (1 - t_{*p}) \int_{\tilde{t}_{*Rb}}^{\tilde{t}_*} \tilde{t}_*^{n_2 - 1}\, d\tilde{t}_* =$$

$$t_{*p}(1 - \tilde{t}_{*Lb}^{n_2} + \alpha_* \tilde{t}_{*Lb}^{n_1}) + \alpha_*(1 - t_{*p}) \tilde{t}_{*Rb}^{n_1} + (1 - t_{*p})(\tilde{t}_*^{n_2} - \tilde{t}_{*Rb}^{n_2}) \tag{3.47b}$$

$$for\ t_{*Rb} \le t_* \le 1,\ T_s > T_b$$

where $\tilde{t}_*$ is as previously defined.

For storm of greater duration than two bursts, the time of peak precipitation intensity is selected by first dividing the total duration into four quartiles. The probability of observed storms that had their peak intensity in the first and fourth quartiles was determined from the intra-storm characteristics routines and summarized by cosine coefficients to capture within-year variations. The probability of peak intensity in the second and third quartiles are

assumed to be equal and calculated by subtracting first and fourth quartile probabilities from one. The time of peak intensity is randomly selected such that the frequency of occurrence in each quartile corresponds to those observed. The time of peak intensity is taken at the midpoint of the quartile.

*Storm Duration*

The theoretical framework of the previous section requires a determination of the storm duration. The user has three options for determining this parameter. The most straightforward option is to assume no relationship with storm depth. The cosine coefficients for the mean and standard deviation of duration are stored in the precipitation file and can be used to predict duration using the normal, log-normal, or extreme value type I distribution. The user can also select a linear relationship between duration and storm depth. The cosine coefficients for the slope and the standard error are also stored in the intra-storm file. The user can select the normal or the extreme value type I distribution to add a random component.

For the logistic duration model, the cosine coefficients for the statistical characteristics of the residuals are stored in the intra-storm file where the residuals are defined by Equation 3.10. By rearranging this equation, the normalized duration is determined as function of the normalized depth ($x^*$ = daily precipitation divided by daily precipitation depth) as

$$y^* = \frac{\beta^*[\exp(\kappa_1^* x^*(1+\beta^*))\exp(-e_d^*(1+\beta^*))-1]}{1+\beta^*\exp(\kappa_1^* x^*(1+\beta^*))\exp(-e_d^*(1+\beta^*))} \tag{3.48}$$

where cosine coefficients are stored in the intra-storm data file for $\beta^*$ and $\kappa_1^*$ and for the mean and standard deviation of $e_d^*$.

*Fraction of Storm Duration with No Precipitation*

The WINDS model also simulates time periods within a storm that has no precipitation. Here the fraction of the storm duration with no precipitation (fraction of gaps) is a critically important parameter. This observed fraction was examined with the intra-storm data.

Although cosine coefficients are available in the intra-storm data file to represent the mean and standard deviation of no-precipitation gap and to represent a linear relationship between no-precipitation gap and duration, the WINDS model uses the exponential relationship shown in Figure 3.6. The current version of the WINDS model does not place a high priority on predicting accurately the no-precipitation gap and compromises this feature to obtain the proper depths within the storm. By using the definition of residuals given by Equation 3.14, the fraction of no-precipitation gap can be predicted as

$$g = 1 - \exp(\kappa^* \, y^*) \, \exp(-e_g^*) \tag{3.49}$$

where cosine coefficients are stored in the intra-storm data file for $\kappa^*$ and for the mean and standard deviation of $e_g^*$. The extreme value type I distribution is used as the distribution for $e_g^*$.

The WINDS model computes cumulated precipitation depth for a fixed storm interval, corresponding to "bursts" of precipitation. The fraction of gaps is only applied if the total storm duration is greater than two bursts. A gap in precipitation is not allowed at the time of peak precipitation intensity and the nearest surrounding bursts. When there is a no-precipitation time interval, the intensity of subsequent bursts is increased to maintain the same total depth. This concept is illustrated in Figure 3.16.

In addition to the fraction of no-precipitation gaps, the persistency trend might also be of interest; that is, the probability that the next time interval within a storm has precipitation is dependent on whether the current time period has rain. A first-order Markov chain is used where the transitional probabilities of wet time period given that the previous time period is also wet and the probability of a wet time period given that the previous time period was dry. These transitional probabilities were determined from intra-storm data, and the results are summarized using cosine coefficients in the intra-storm file.

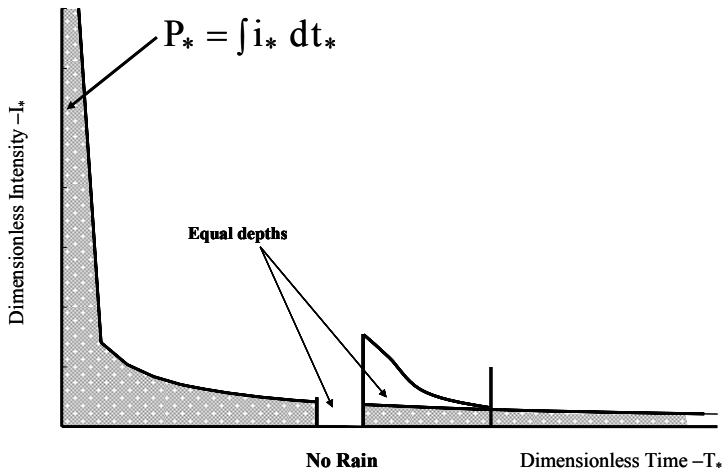


Figure 3.16. Impact of No-Precipitation Gap on Intensity.

The transitional probabilities obtained from cosine curves are adjusted to place additional or fewer no-precipitation gaps during the simulation of the storm pattern. This adjustment is shown in Figure 3.17. In this figure, $N_g$ and $n_g$ are the total number of no-precipitation time periods necessary to achieve the overall fraction of no-precipitation gaps and the current count of no-precipitation time periods, respectively; $N_b$ and $n_b$ are the total and current number of time periods for the storm. The x-axis is then the ratio of the remaining time periods needed to achieve the overall no-precipitation gap and the total remaining time periods. If this ratio is zero, then all the time periods for no-precipitation gaps have been used. The probability of obtaining another no-precipitation gap is then set to zero preventing any more no-rain gaps. If the x-axis value is one, all of the remaining time periods must be no-precipitation gaps and therefore the transitional probabilities are set to one. Breakpoints in the curves correspond to the transitional probabilities that are determined from the cosine coefficients. They correspond to the transitional probabilities at the beginning of the storm.

For a small storm duration of only two storm bursts, the WINDS model distributes the depth among the two bursts based on the fraction of the total precipitation for two burst storms analyzed from the intra-storm data file. Cosine coefficients are used to represent within-year variations, and these coefficients are stored in the intra-storm file.

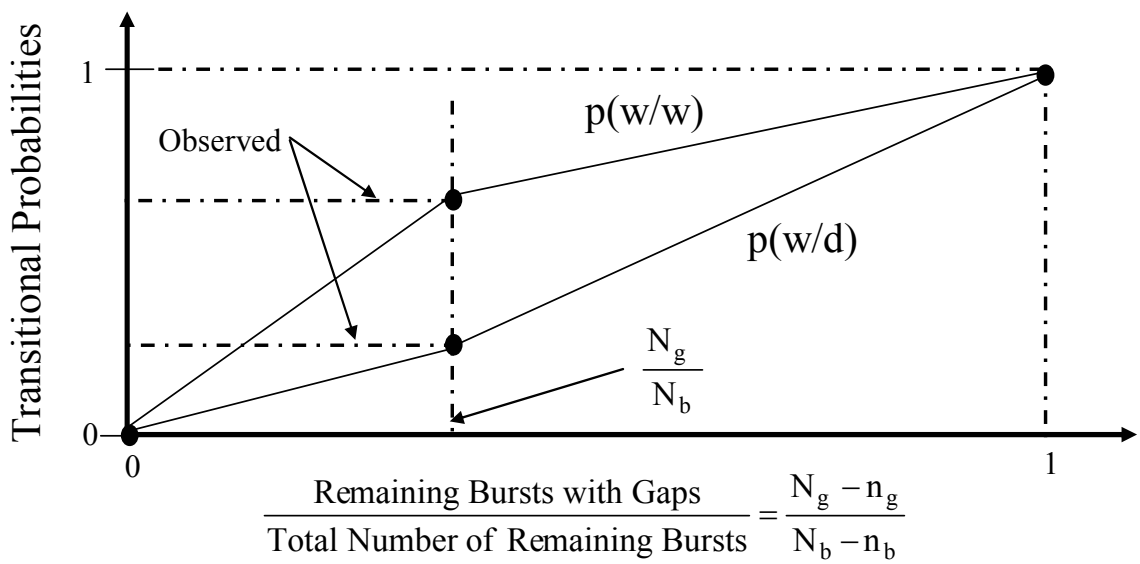


Figure 3.17. Changes in Transitional Probabilities within Storms.

## Additional Features

One of the advantages of using normalized statistics for the mean and standard deviation for the weather variables is that it allows the WINDS model to more easily adjust predicted values for locations whose weather differs from that of the nearest climate/intra-storm station. For example in mountainous terrains, temperature varies with elevation, and therefore temperatures corresponding to climate station at a low elevation do not correspond to those of a location at a higher elevation. Although it is unlikely that an adequate time series data set exists at the higher elevation for determining the parameters of the WINDS model, the user will often have sufficient information to estimate the annual mean temperature and possibly the standard deviation. The user has the option of changing the $X_{std}$ normalizing statistics of Equation 3.24 to the mean and/or standard deviation of the study location. The WINDS model will then simulate daily climate variables to correspond to the mean (and possibly standard deviation) at the study location. Trends of the weather variable relative to its normalizing value are the same as that of the climate station. Radiation is latitude dependent. Therefore, in addition to changing the mean and standard deviation, the user can improve the simulation of radiation by specifying the latitude for his/her location.

The primary goal in the development of the WINDS model was to predict different weather scenarios for a particular year. Nonetheless, the WINDS model can also be used to predict weather in future years. Another advantage of using normalizing statistics is the ease in which climate change can be simulated. For this type of application, the $X_{std}$ normalizing statistics of Equation 3.24 are simply allowed to vary with year of simulation. The user can vary both the mean and standard deviation $X_{std}$ with year. The following equation is used in the WINDS model.

$$X_{t,std}(year) = X_{std}[1 + F_{\exp}(year) + F_{\sin}(year) + F_{lin}(year)] \tag{3.50}$$

where $X_{t,std}$ is the varying normalizing coefficient with year of simulation that can be determined as the sum of an exponential function, a periodic sine function, and/or a linear function. These functions are defined as

$$F_{\exp}(year) = A_{\exp,\max}(1 - \exp(-B_{\exp,rate} year)) \tag{3.51a}$$

$$F_{\sin}(year) = A_{\sin,\max} \sin\left(\frac{year - 1}{B_{\sin,per}}\right) \tag{3.51b}$$

$$F_{lin}(year) = B_{lin,slope}(year - 1) \tag{3.51c}$$

where the A and B coefficients are entered by the user. The determination of these coefficients is not a trivial task. The functions in Equation 3.50 can be set to zero by using zero A coefficients or $B_{lin,slope}$ coefficients. The above equations are applied to both the mean and standard deviation of the weather variables.

Five-day weather forecasts are frequently available and the user may wish to use these forecasts in the simulations of different weather scenarios. The mean and standard deviation values obtained from the cosine function for the non-precipitation variables are overridden by five day forecast information provided by the user. Forecast expected value is taken as the mean value and the possible range in value is used to estimate the standard deviation. Standard deviations are defined to increase from the first day to the fifth day of the forecast. The percent chance of rain is used to override the probability of wet day given a dry day and the probability of a wet day given a wet day.

# *Chapter Four*
# *Modeling Algorithms of the WATER Model*

## Introduction

Assessment of the effectiveness of sediment control practices requires that the weather predicted from the WINDS model be used to simulate the runoff and erosion from hillslopes. Important hillslope processes are shown in Figure 4.1. They include surface runoff processes of which infiltration and overland flow are particularly important, plant processes related to plant growth and evapotranspiration, and erosion and sediment transport that include detachment by raindrop impact and shear forces from surface flows. At the toe of the hillslope, sediment deposition is common and occurs when the sediment load exceeds the transport capacity of the flow.

The WATER model has more than one algorithm to simulate the key components. The selection of the best algorithm is closely tied to the availability of their parameters and the expertise of the user. Since the parameter sets for construction site is quite limited, the best modeling algorithms will often not be the most theoretically appealing. However as future studies provide greater insight into processes and a larger data base is established, the selection of the best modeling algorithms will likely move to more rigorous process-based relationships.

The description of the algorithms in the WATER model is divided into those used for runoff processes, plant processes, and erosion and sediment transport. Prediction of runoff processes is largely dependent on the methods to predict infiltration, surface depressional storage, and overland flow. Important algorithms for plant processes are those used to predict plant growth and evapotranspiration. Three different levels of modeling rigor are used for erosion and sediment transport. The simplest methods are those based on the Universal Soil Loss Equation (USLE). More process-based methods based on the approach of the Water Erosion Prediction Project (WEPP) model are available to the user. The most rigorous algorithms, but the least tested, are based on recent work done at the University of

Minnesota.

Estimation of soil parameters is an important component in modeling runoff and erosion from construction sites. A separate class is used to estimate these parameters. Different algorithms were selected to allow the user to select the best method given the information available for his/her design. Routines have been developed to predict matrix potential and relative conductivity using Brooks-and-Corey (1964) and van Genuchten (1980) relationships and other soil parameters such as porosity, residual moisture content, bubbling pressure, pore size distribution, moisture content at field capacity, moisture content at wilting point, and saturated conductivity. Estimates of these later parameters can be obtained using the mean values by soil texture of Rawls et al.'s (1989) data set of more than 5000 samples. Predictive equations proposed by Rawls et al. and developed for the WEPP model (Flanagan and Nearing, 1995) is also available to users.

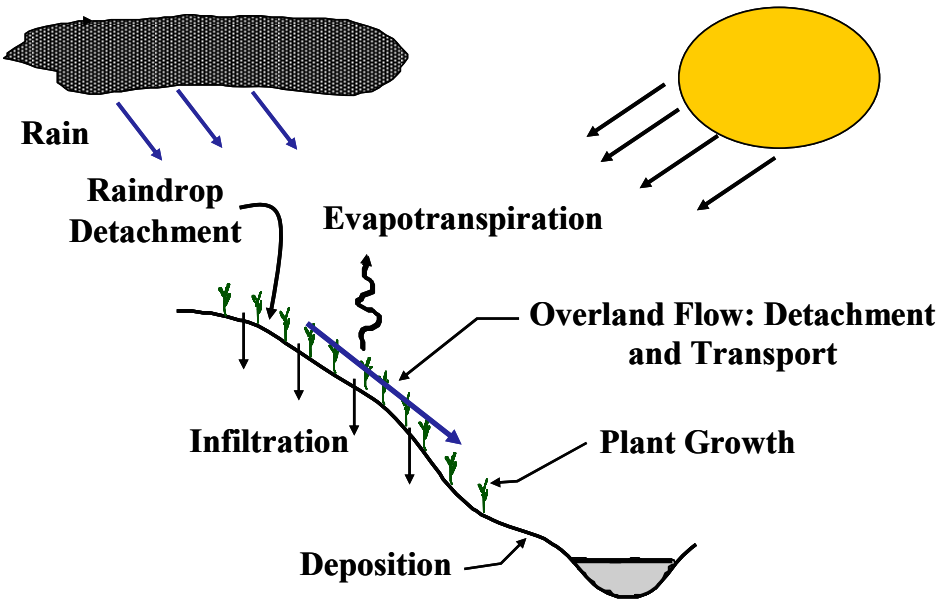


Figure 4.1. Important Hillslope Processes for the WATER model.

## Runoff Processes

*Infiltration and Surface Depressional Storage*

Infiltration is a critical component of the runoff processes because it divides rainfall into surface and subsurface flow paths. A number of different infiltration methods has been coded and is available to the user. These methods are (1) Green-Ampt-Mein-Larson (GAML) infiltration model (Mein and Larson, 1973), (2) two-layered GAML model, (3) dual-porosity GAML model, (4) Holtan infiltration method (Holtan, 1961), (5) Horton infiltration equation equation (Horton, 1939), (6) infiltration based on the curve number method (SCS, 1972; Hjelmfelt, 1980), and (6) constant infiltration rate of the phi-method. Once again, the selection of the best infiltration method is dependent on the type of problem and availability of parameters. Only information on the GAML model and the curve number method is summarized here.

The Green-Ampt's infiltration equation is based on the idealized moisture content profile of box shape corresponding to sharp wetting front. The infiltration rate is defined as

$$f = K_s \left( \frac{(\theta_s - \theta_i)\psi_f + F}{F} \right) \tag{4.1}$$

where f is the infiltration rate, $K_s$ is the effective saturated conductivity, $\theta_i$ and $\theta_s$ are the initial and effective saturated moisture content, respectively, $\psi_f$ is the average suction at the wetting front and F is the cumulative infiltration depth. Cumulative infiltration depth is predicted as

$$F = F_s + (\theta_s - \theta_i)\psi_f \ln\left( \frac{(\theta_s - \theta_i)\psi_f + F}{(\theta_s - \theta_i)\psi_f + F_s} \right) + K_s(t - t_s) \tag{4.2}$$

where $F_s$ and $t_s$ are the infiltration depth and time at effective surface saturation. Mein and Larson (1973) used the Green and Ampt's approach to estimate $F_s$ as

$$F_s = \left( \frac{(\theta_s - \theta_i)\psi_f}{(i / K_s) - 1} \right) \tag{4.2}$$

where i is a constant rainfall intensity. For constant rainfall intensity, $t_s$ is obtained by simply dividing $F_s$ by i. In the WATER model, the Mein and Larson's approach is modified for unsteady rainfall intensity using the concepts given by Chu (1978). Li et al.'s (1976) simple two-step method is used to solve the GAML model efficiently. The GAML model is only

used when the rainfall intensity is greater than the infiltration capacity given by Equation 4.1. If the rainfall intensity is less than the infiltration capacity, the infiltration rate is taken as the rainfall intensity.

Abstraction is the removal of rain from surface runoff processes. In addition to infiltration, it includes surface depressional storage and vegetative interception, of which surface depressional storage is of greater importance. Initial abstraction is the surface depressional storage, vegetative interception and infiltration ($F_s$ for the GAML model) prior to the start of runoff. Most of the total surface depressional storage and vegetative interception occur prior to runoff. Rainfall excess depth is defined as the difference between rainfall and abstraction depths. Excess depths drive the detachment and transport of sediment by surface runoff.

Simple vegetative interception models are used in the WATER model where the user specifies whether the relative interception depth as large, medium or small. Adjustments for wind speed are also possible. Two methods for surface depressional storage are available to the user. The simplest approach is to specify whether the relative depth is large, medium, or small. A more rigorous model is available using the results of Onstad's (1984). Surface depression storage depth is then predicted as function of the roughness and slope of the surface by the following equation.

$$SS_d = R_r\ (0.112 + 0.031R_r - 0.012S_L) \tag{4.3}$$

where $SS_d$ is the surface depressional storage (mm), $R_r$ is the roughness of the surface and $S_L$ is the slope of the land.

The curve number method is a two stage model that directly predicts rainfall excess. If the cumulative precipitation depth is less than initial abstraction, then the excess depth is zero. If the cumulative precipitation depth is greater than initial abstraction, the excess depth is predicted as

$$Z = \frac{(P - I_a)^2}{P - I_a + S} \qquad if\ P > I_a \tag{4.4a}$$

where Z is the cumulative excess depth for a cumulative precipitation depth P, $I_a$ is the initial abstraction, and S is a maximum abstraction depth related to a curve number (CN) by

$$S = \frac{1000}{CN} - 10 \tag{4.4b}$$

The user can specify an initial abstraction depth, estimate the initial abstraction from vegetative interception and surface depressional storage method previously discussed, or use the default value in the NRCS curve number method where

$$I_a = 0.2\ S \tag{4.4c}$$

*Overland Flow*

As excess water travels over the surface, it combines with water from other areas to increase the volumetric flow rate. As the rate increases, the ability of the flow to detach and transport particles also clearly increases. The user is given several unit hydrograph options and four kinematic wave approaches. Unit hydrograph theory is used to predict flow rate assuming (1) a linear reservoir, (2) a series of linear reservoirs, (3) a time-area curve coupled with a linear reservoir, (4) a linear reservoir for surface runoff and a linear reservoir for channel processes, and (5) time-area-excess-depth curve linked with a linear reservoir. The kinematic wave options are based (1) equilibrium flow response, (2) constant excess intensity response, (3) general numerical solution for rectangular surface, and (4) general numerical solution for a converging surface. The first two kinematic wave options are only recommended for small drainage areas.

Unit hydrograph theory is a conceptual modeling approach widely used to predict surface runoff. A unit hydrograph is defined as a hydrograph of one unit of surface runoff, usually for specific duration. The approach can be applied to a watershed scale that includes both overland and channel flow processes. Unit hydrographs were originally defined using observed data, but the theory has been expanded to include process-based concepts. The following notation is used here: $\Delta t$ is the duration of rainfall excess burst, DUH is the unit hydrograph for storm burst of $\Delta t$, IUH is the instantaneous unit hydrograph corresponding to $\Delta t \rightarrow 0$, $\Delta Z$ is the rainfall excess depth for storm burst defined as the product of rainfall excess intensity ($i_e$) and $\Delta t$, and Q is the flow rate of runoff hydrograph.

Unit hydrograph theory is based on properties inherent in linear differential equations. One of these relationships is the principle of proportionality that states that the flow rates are proportional to excess depths. Another important relationship is the principle of superposition. This principle allows a complex input to be divided into simpler components and then solving these simpler components to determine solution for the original complex input. For runoff, the principle of superposition allows the flow rate to be determined using the convolution integral defined as

$$Q(t) = \int_0^t IUH(t - \tau) i_e(\tau)\, d\tau \tag{4.5}$$

where $i_e$ is the rainfall excess intensity which is known from the rainfall hyetograph infiltration and surface depressional storage relationships of the previous section. The WATER model allows the user to select several different instantaneous unit hydrographs (IUH).

A numerical solution to Equation 4.5 is shown in Figure 4.2 for three bursts of excess. Each burst resulted in a runoff hydrograph. These runoff hydrographs are lagged and added to determine the overall response.

Kinematic wave approach is based on the coupling of the conservation of mass with the equation of motion with negligible inertial term and pressure forces. It assumes broad sheet flow for overland conditions. The kinematic wave solution for these conditions can be written as

$$\frac{\partial q}{\partial x} + \alpha \beta q^{\beta-1} \frac{\partial q}{\partial t} = i_e \tag{4.6a}$$

where q is the flow rate per unit width and $\alpha$ and $\beta$ are parameters defined from a rating curve or from Manning's equation. For Manning's equation, $\beta = 3/5$ and $\alpha = [n/(1.49 S_L^{1/2})]^{\beta}$, where n is Manning's n and $S_L$ is land slope. In the WATER model, the following approximation is used to solve the above equation (Chow et al., 1987)

$$q_{i+1}^{j+1} = \frac{q_i^{j+1}(\frac{\Delta t}{\Delta x}) + \alpha\,\beta\, q_{i+1}^{j}(\frac{q_{i+1}^{j+1} + q_{i+1}^{j}}{2})^{\beta-1} + \Delta t(\frac{i_{ei}^{j+1} + i_{ei+1}^{j}}{2})}{\frac{\Delta t}{\Delta x} + \alpha\,\beta(\frac{q_{i+1}^{j+1} + q_{i+1}^{j}}{2})^{\beta-1}} \tag{4.6b}$$

where i and j are grid locations in x and t, respectively. Checks are used for the special case of no flow on the surface.

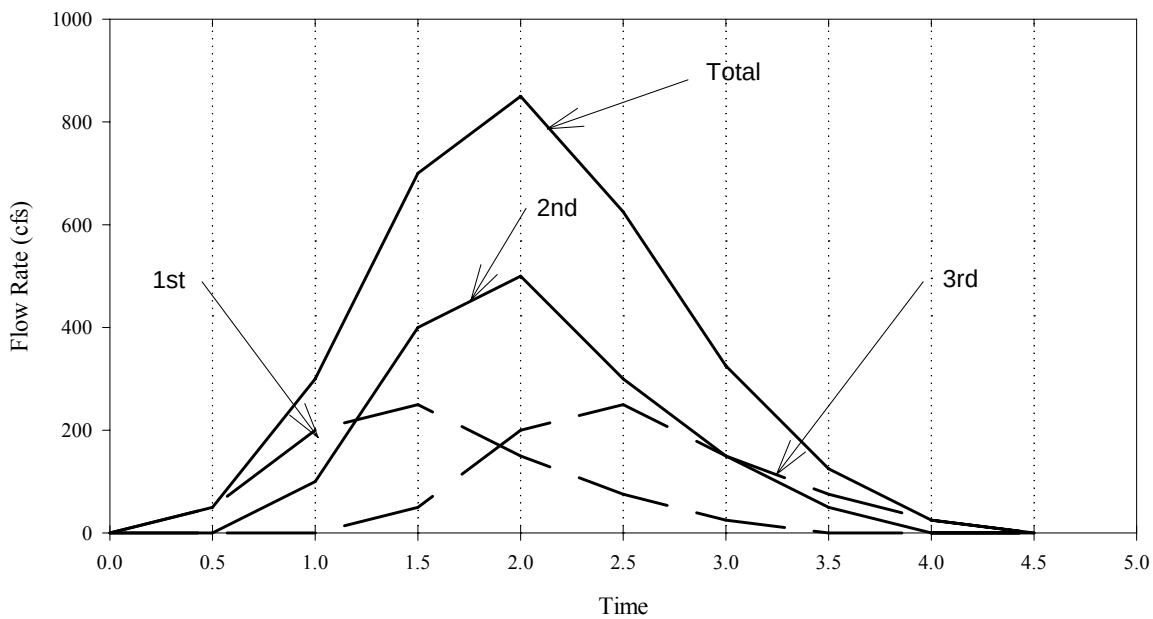


Figure 4.2. Numerical Solution to the Convolution Integral for Three Rainfall Excess Bursts.

## Plant Processes

### *Plant Growth Modeling*

Plant growth at construction sites provides vegetative cover for erosion control and leaf canopy that influences evapotranspiration. Plant models are commonly used for agricultural crops (Wilson and Jamieson, 1984; Jones et al., 1986). Generally, for these applications, competition among different types of plants is relatively unimportant. Weeds are controlled by effective management practices. However for many construction sites, the establishment of any vegetation is often important in reducing erosion. Less interest lies in the growth of a

particular plant species

Two general approaches are available in the WATER model to simulate plant growth. The simplest approach uses empirically derived biomass curves for a community of plants. The accuracy of this approach is dependent on available data for the plant community at a given construction site. The other approach is more rigorous and uses concepts from crop growth models.

The process-based modeling approach represents the potential plant community at a site by several different plant groups. Germination and other growth stages are triggered by heat unit indices. The triggering heat unit indices vary among the plant groups. Prior to reaching maturity, potential daily biomass for each plant group is estimated using the photosynthetic active radiation. Observed biomass as a function of photosynthetic active radiation for eleven different crops is shown in Figure 4.3. The potential biomass for any given day is obtained as

$$b_{mT} = 0.02092\, P_{bm}\, R_s\, (1 - \exp(-0.65\, LAI_T)\,] \tag{4.7}$$

where $P_{bm}$ is a plant factor for converting photosynthetic active radiation, $R_s$ is the solar radiation obtained from the WINDS model, and $LAI_T$ is the leaf area index. A larger leaf area provides more available energy for plants to grow. After plant maturity, different set of relationships are used to consider the biomass of the plant community.

Equation 4.7 allows the potential biomass to be estimated. Adjustments in this potential biomass are necessary for non-optimal conditions at construction sites. As an example, the reduction in the photosynthetic rate as a function of an air-temperature stressor is shown in Figure 4.4. In the WATER model, reduction in optimal biomass is done for the following stressors: (1) seed availability, (2) soil moisture availability, (3) availability of nitrogen, (4) availability of phosphorous, (5) air temperature, and (6) leaf area competition among plant groups. The impact of all of these stressors are represented by the general relationship

$$k_s = 1 + c\,(\hat{S}_f - \hat{S}_{fopt})^2 \tag{4.8a}$$

where $k_s$ is the stressor factor, c is a definable factor that depends on a minimum or

maximum limit for $k_s$, $\hat{S}_f$ is a normalized stressor defined as

$$\hat{S}_f = \frac{S_f}{1+\kappa(S_f - S_{fm})/S_{fopt}} \tag{4.8b}$$

where $S_{fm}$ is the stressor value where $k_s$ equal zero, $S_{fopt}$ is the stressor value where $k_s$=1 and κ is asymmetrical adjustment factor. The parameters of the stressor equation are shown in Figure 4.4 using the general form of $y = y_{min} + (y_{max}-y_{min})k_s$, where $y_{min} = 0$.

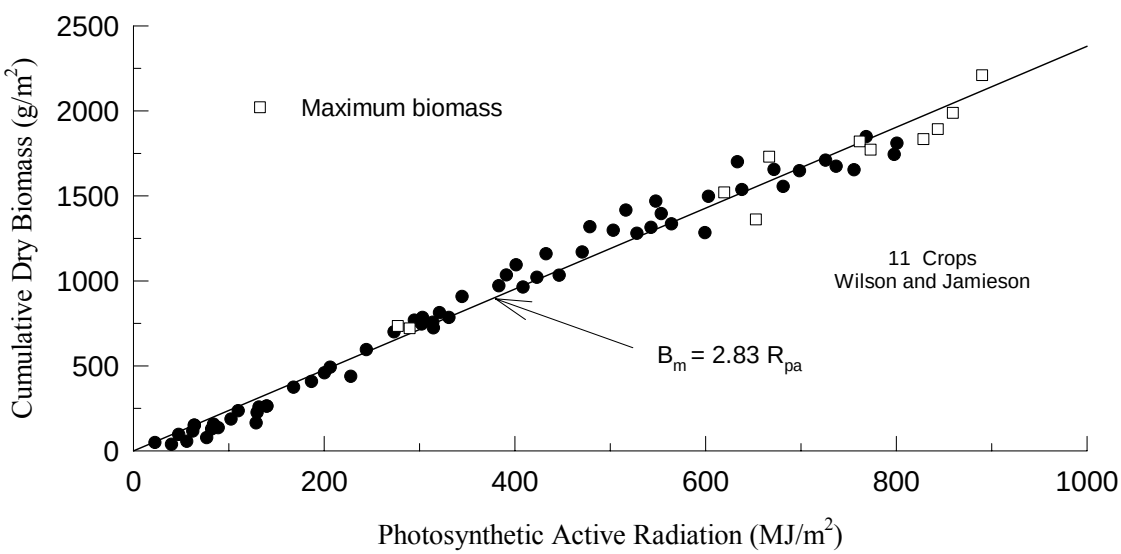


Figure 4.3. Relationship between Biomass and Photosynthetic Active Radiation.

The application of these concepts to a plant community of different plant groups is shown in Figure 4.5. Total biomass and leaf area index is first computed for the entire plant community. This total biomass is then distributed among the different plant groups. Each plant group has a unique set of phenological properties (such as early emergence), efficiency of biomass conversion, and stressor properties (such as tolerance to low soil moisture content). Plant groups that have characteristics that are best suited to site conditions receive a greater fraction of the total biomass. This competition among plant groups determines the dominate plant group.

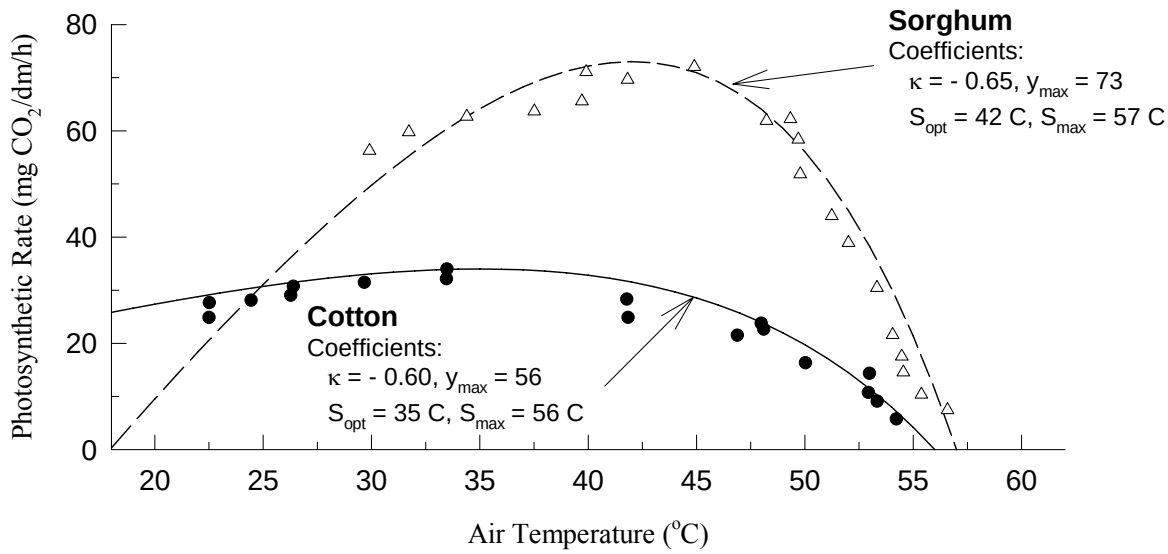


Figure 4.4 Plant Stress as Function of Air Temperature.

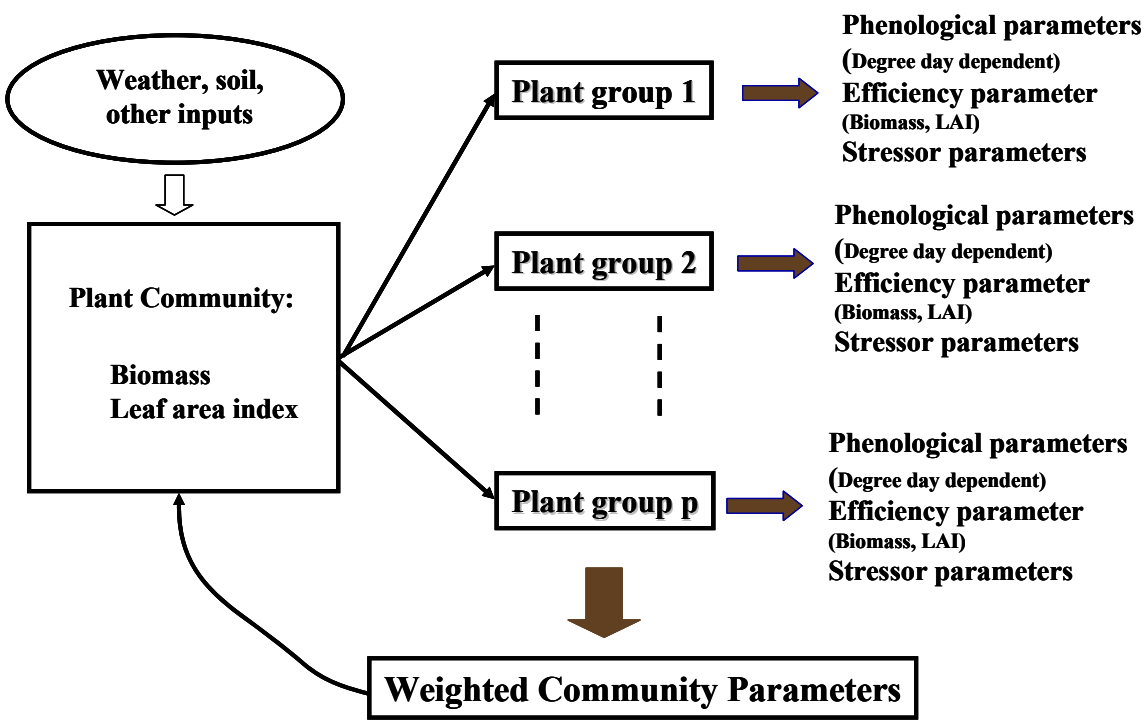


Figure 4.5. Computations for a Community of Plant Groups.

*Evapotranspiration*

.

Evapotranspiration is a critical process for determining the moisture content of the soil, which is used for computing infiltration for individual storms and for simulating plant growth. Users have a choice for predicting potential ET using pan evaporation, Priestly-Taylor, Penman and Penman-Monteith methods (Jansen et al., 1990). Crop coefficients and the leaf-area index method are used to estimate potential ET for site conditions (Burman et al., 1983; Ritchie and Barnett, 1971). The impact of water availability in the soil is modeled using either the simple linear relationships proposed by Larson (1985) or by using relationships that relate leaf resistance to soil moisture potential. Only the more rigorous of these options will be presented here.

The Penman-Monteith method is based on an energy balance for a plant canopy. Important energy terms are shown in Figure 4.6. The net radiation, $R_n$, is defined as the net radiation into the plant canopy and can be estimated by coupling the solar radiation from the WINDS model with albedo and other factors. Net radiation is the dominate energy term for the control volume. The sensible heat flux, $H_s$, is defined as the net heat flux leaving the canopy as the result of temperature difference, primarily through a plane located at the top of the canopy, but possibly also by the net advected heat term. Sensible heat is an important energy term. The sensible heat flux, G, is defined as the net heat flux leaving the plant canopy to the soil. Although some researchers/modelers consider G for short time steps (less than a day), it is usually small when integrated over an entire day. The latent heat, RET, is defined as the heat used for evapotranspiration for a reference crop. The rate of change in energy of the canopy, $\Delta S$, is typically negligible. Other negligible energy terms are the viscous dissipation work and biological (non-RET) and chemical activities.

By using the slope of the saturation vapor pressure-temperature curve to approximate the temperature of the leaf surface, by neglecting insignificant energy terms shown in Figure 4.6, and by using resistance-type of relationships for heat and vapor movement, the Penman-Monteith method can be derived as

$$RET = \left(\frac{\Delta}{\Delta + \gamma_c (1 + r_{lv} / r_{ah})}\right)(\mathrm{R_n} - G) + \left(\frac{\rho c_p}{\Delta + \gamma_c (1 + r_{lv} / r_{ah})}\right)\left(\frac{e_a^s - e_a}{r_{ah}}\right) \tag{4.9}$$

where $\Delta$ is the slope of the saturation vapor-pressure-temperature curve, $e_s$ is the saturated vapor pressure, $e_a$ is the vapor pressure ($e_a = e_a^s$ rh), $\rho$ is the air density, $c_p$ is the specific heat at constant pressure, $\gamma_c$ is the psychrometric constant, and $r_{lv}$ and $r_{ah}$ are the stomatal resistance and heat-atmospheric resistance, respectively. The heat-atmospheric resistance can be derived from turbulent flow theory for log-velocity profiles as

$$r_{ah} = \frac{[\ln(\frac{z-d}{Z_h}) - \psi_h][\ln(\frac{z-d}{Z_m}) - \psi_m]}{\kappa_v^2 U(z)} \tag{4.10a}$$

where $\kappa_v$ is the von Karmon constant and U(z) is the velocity measured at a height of z. The remaining parameters are dependent on the type of plant. For a reference crop of alfalfa, the stomatal resistance can be estimated as (Jansen et al. 1990)

$$r_{lv} = \frac{100}{0.5\, LAI} \qquad where\ \ LAI = 2.5\ln(h) - 1.4 \tag{4.10b}$$

and $\psi_h = \psi_m = 0$, $Z_m = 0.123$ h, $Z_h = 0.1\ Z_m$, and d=0.67 h, where h is the canopy height.

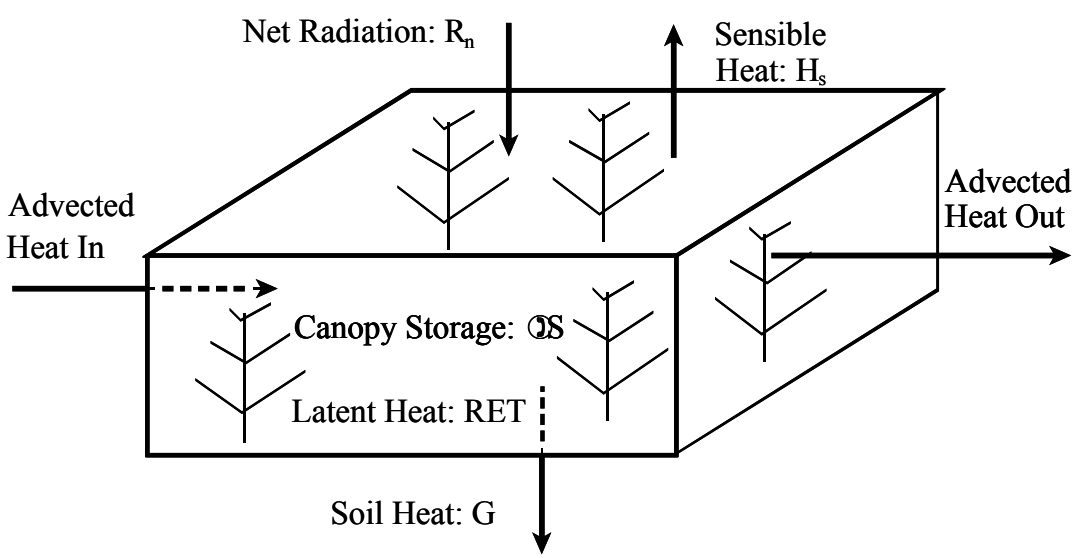


Figure 4.6. Energy Balance for Plant Canopy.

Potential evapotranspiration for the reference crop of alfalfa is predicted by Equation 4.9 for the parameters as defined by Equation 4.10b. This potential evapotranspiration needs to be adjusted to consider other plant types at different stages of growth. In the WATER model, the adjustment factor can be determined from standard growth curves or by using the leaf area index. The leaf area index is characteristic of the plant community predicted by the plant growth algorithms. The ratio of potential plant transpiration and RET as a function of the leaf area index is shown in Figure 4.7. For LAI < 3, this ratio is predicted in the WATER model as

$$\frac{T_p}{RET} = 0.52\sqrt{LAI} \qquad for \quad LAI < 3 \tag{4.11}$$

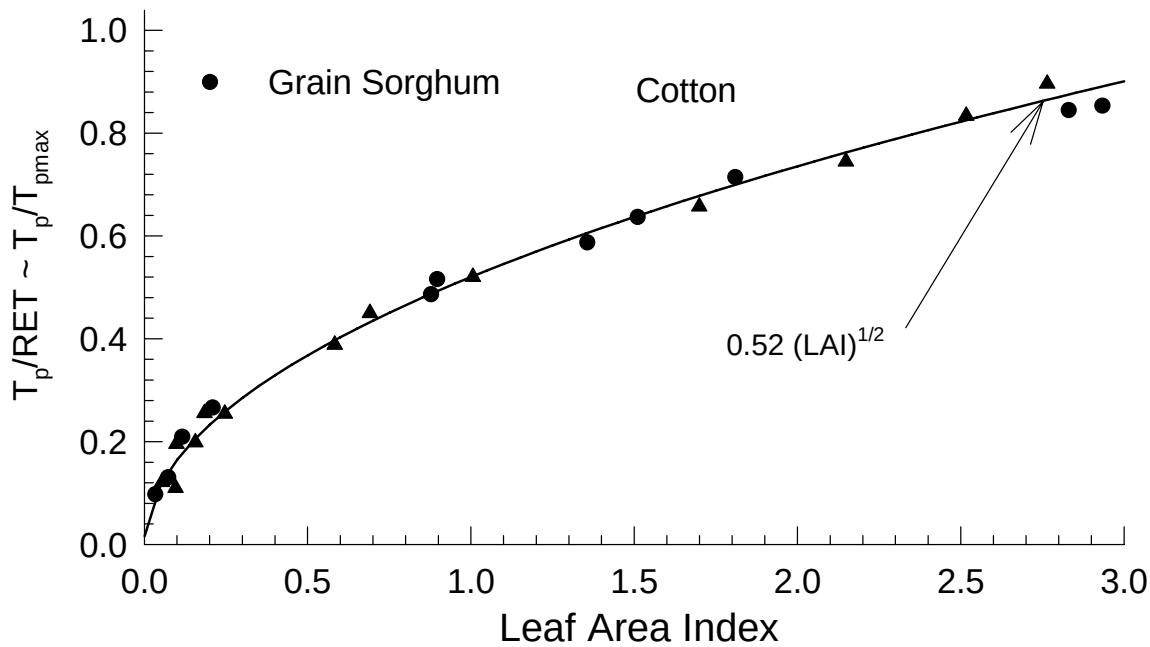


Figure 4.7. Potential Transpiration Ratio as Function of Leaf Area Index.

Actual evapotranspiration is less than potential evapotranspiration when there is insufficient water in the soil matrix. One approach in the WATER model for predicting this reduction is based on the potential difference between the soil matrix and the plant leaf. As discussed by Campbell and Norman (1998), the relative humidity inside the leaf stomata is nearly one,

even under stressed conditions. The leaf is therefore unable to control transpiration by substantially dropping its leaf potential. Reduced transpiration can, however, be obtained by closing its stomata (increasing leaf resistance). Figure 4.8 shows changes in leaf resistance as a function of leaf potential. Also shown in this figure are the mathematical approximations used in the WATER model to represent leaf resistance.

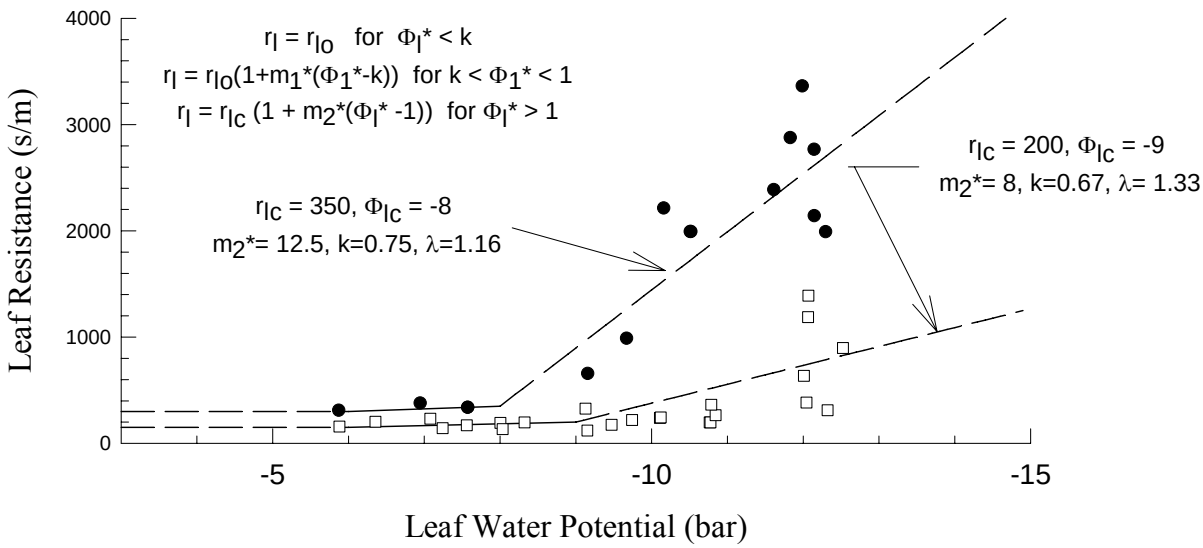


Figure 4.8. Leaf Resistance as Function of Leaf Potential.

By using the relationships shown in Figure 4.8, Brooks-and-Corey relationship for soil matrix potential and considerable algebraic manipulation, the ratio of actual transpiration to the potential transpiration (without water stress) can be defined as

$$\frac{T}{T_p} = \frac{\sqrt{(\mathrm{km}_1^* - 1 + \mathrm{m}_1^*\Phi_s^*)^2 + 4\mathrm{m}_1^*[k + (1 - k\mathrm{m}_1^*)\Phi_s^*} - 1}{2\mathrm{km}_1^*} + \frac{1}{2} - \frac{\Phi_s^*}{2k} \quad for\ A_{wc} \le A_w \qquad (4.12a)$$

$$\frac{T}{T_p} = \frac{\sqrt{(\mathrm{m}_2^* - 1 + \mathrm{m}_2^*\Phi_s^*)^2 + 4\mathrm{m}_2^*[(k/\lambda) + (1 - \mathrm{m}_2^*)\Phi_s^*} - 1}{2\mathrm{m}_2^*} + \frac{1}{2} - \frac{\Phi_s^*}{2k} \quad for\ A_w \le A_{wc} \qquad (4.12b)$$

where $A_w$ is the available water in the soil, $A_{wc}$ is a breakpoint available water value, $\Phi_s^*$ is a dimensionless soil potential, and k, $m_1^*$, $m_2^*$, and $\lambda$ are leaf resistance parameters as shown in Figure 4.8.

## Erosion and Sediment Transport

*USLE-based Routines*

The Universal Soil Loss Equation (USLE) was developed as a tool for soil conservationists to use for developing farm management plans to control erosion and maintain soil productivity from agricultural lands. It is best suited to predict average, annual soil loss. An advantage of the USLE-based approaches is the relatively large data set used to determine erosion parameters. The USLE is based on more than 10,000 plot-years of data. Substantial efforts were undertaken to improve the prediction accuracy of the original USLE resulting in the Revised Universal Soil Loss Equation (RUSLE). Of particular interest with this modification is the calculation of the slope length coefficient as a function of a rill-to-interrill erosion parameter.

One of the erosion modeling algorithm in the WATER model is the modified Universal Soil Loss Equation (MUSLE) (Williams, 1977). This method was developed for storm events. It replaces the rainfall factor in USLE with a runoff factor that was evaluated using 778 storms with a variety of different watersheds. The MUSLE predicts total sediment yield from the construction site. Sediment yield is predicted by the following equation

$$Y = 95(V\,Q_p)^{0.56}\,K\,L\,S\,C\,P \tag{4.13}$$

where 95 $(VQ_p)^{0.56}$ is the runoff erosion factor, Y is the sediment yield at the outlet, V is the volume of runoff, $Q_p$ is the peak flow rate and where K, L, S, C, and P are the USLE factors for erodibility, slope length, slope steepness, cover and practice, respectively.

The USLE-based method of SLOSS (Wilson et al, 1982) is also available to the user of the WATER model. With this method the detachment is divided into interrill and rill components, where the USLE rainfall erositivity is used to compute detachment from interrill areas and the volume and peak flow rate is used to determine detachment from rill areas. Deposition is computed if the sediment load in rills exceeds the transport capacity of the flow. The transport capacity of the flow is computed using Yang's unit stream power

equation (Yang, 1973).

*WEPP-based Routines*

The Water Erosion Prediction Project (WEPP) was developed as an alternative, more process-based approach to USLE for predicting annual average erosion from agricultural lands (Flanagan and Nearing, 1995). The overall framework for this project is similar to that used by the WATER model. Erosion in the WEPP model is divided into interrill and rill components. In contrast to the SLOSS approach, the parameters for the WEPP modeling approach are not based on the USLE data set.

The WEPP-based form of interrill detachment used in the WATER model is

$$D_i = K_i \; i^2 \; C_i \; G_i \tag{4.14}$$

where $D_i$ is the interrill detachment, $K_i$ is the interrill soil erodiblity, i is the effective rainfall intensity, $C_i$ and $G_i$ are the interrill canopy and ground cover factors. The rill detachment by surface runoff is estimated as

$$D_r = K_r \; (\tau - \tau_c) \; (l \, WP) \; (1 - \frac{G_d}{T_c}) \qquad for \; \tau > \tau_c \tag{4.15}$$

where $D_r$ is the rill detachment rate, $K_r$ is the rill erodibility, $\tau$ is the bed shear defined as $(\rho gRS)^{1/2}$, $\tau_c$ is the critical bed shear, l is the length of the rill, WP is the wetted perimeter, $G_d$ is the downslope sediment load, and $T_c$ is the transport capacity of the flow. A simple mass balance is maintained in the rill to estimate $G_d$. This mass balance can be used to compute deposition in the toe area of a typical hillslope. The WEPP-based algorithms assume a fixed number of rills per unit area, corresponding to a set of parallel rills for a given hillslope.

*University of Minnesota's Algorithms*

The third set of erosion modeling algorithms available to the user is based on methods developed at the University of Minnesota in the early 1990s. These algorithms were developed to improve the prediction of detachment by surface runoff. Instead of the fixed number of rills approach used in the WEPP-based methods, the University of Minnesota's

algorithm uses a dendritic network of rills (Wilson, 1991). This approach is based on an analysis of the link characteristics of small-scale surface drainage networks measured from erosion plot data. Networks are predicted by combining link characteristics with the topology defined by an infinite topologically random network. Power relationships are used to describe the shape of rills that are allowed to expand with drainage area.

Wilson (1993) proposed a fundamentally-based flow detachment model that is also available in the WATER model. This detachment model provides a framework for isolating flow from soil characteristics. Flow characteristics are estimated using turbulent detachment forces at the boundary. Turbulent characteristics are represented by the extreme value type I probability density functions. In contrast to the WEPP-based models, the role of sediment load on particle detachment is obtained by the suppression of turbulence by suspended sediment.

# *Chapter Five*
# *Summary and Conclusions*

The WATER (Watershed Assessment Tool for Environmental Risk) model was developed to be a tool to assess the effectiveness of different sediment control practices. Determination of parameters and rigor of modeling approaches are important factors in the development and use of models. Rigorous models typically have many parameters that are frequently unknown. Application of these models to a particular site is then difficult. Overly simple models may have few parameters but are unable to capture important components of erosion and sediment transport. The effectiveness of alternative sediment control practices is then not adequately modeled. Models of erosion and transport of sediment from construction sites need to be sufficiently rigorous to allow sediment control practices to be evaluated and to have parameters that can be determined for site conditions.

The risk assessment is performed with the WATER model by simulating many years of different weather conditions at the construction site for different sediment control plans. Therefore the WATER model needs to adequately represent the weather conditions, the runoff characteristics, erosion processes, and plant growth. In addition, the WATER model needs a user-friendly interface. From the many years of different weather conditions, probabilistic inferences are possible for each of the sediment control options.

A particularly important component of the WATER model is the prediction of daily climate conditions and storm characteristics. The prediction of these characteristics is done using the WINDS (Weather Input for Nonpoint Data Simulations) model. The development of the WINDS model was done in two steps. First, the statistical characteristics of historic weather records were analyzed. Separate routines were developed to efficiently determine the many parameters that were derived from the observed data sets. These routines were used to analyze daily climate variables as well as intra-storm characteristics from 15-minute precipitation data. Within-year variations of key statistics were represented by coefficients of a fitted cosine function. Data from more than 200 climate and 200 15-minute precipitation stations have been evaluated and are available for use by the modeler.

The second step in the WINDS model development was the implementation of algorithms to predict future weather conditions with, ideally, similar statistical properties of those observed. The user has several options in the simulation of weather including different response for wet and dry days, cross correlation among weather variables, incorporation of 5-day forecast information, and different probability density functions for representation of different weather variables. The prediction of intra-storm characteristics is especially important for modeling erosion from small construction sites. A hyetograph method was developed based on DDF (Depth-Duration-Frequency) curves. Important parameters for this method include the storm duration, fraction of total duration without precipitation, and the coefficients of the DDF curve. A comparison of predicted weather and storm characteristics with those observed was very good.

The WATER model has three major components for representing hillslope processes. They are: (1) surface runoff, (2) plant processes, and (3) erosion and sediment transport. Since there is no one best modeling approach for all sites, the WATER model allows the user to select different modeling algorithms for most of these processes. Noteworthy approaches for infiltration are the curve number method and the GAML (Green-Ampt-Mein-Larson) model. The user has choice between unit hydrograph theory and kinematic wave solutions for overland flow. A simple empirical approach and process-based algorithm are available to the user for simulating plant growth. Penman-Monteith method is the most rigorous of the approaches available to predict reference crop evapo-transpiration. Relationships are used to account for different types of plant groups and for water availability in the soil. Algorithms for erosion and sediment transport range from the relatively simple USLE-based approach to the more recent erosion work developed at the University of Minnesota.

## References


Arnold, J.G., J.R. Williams, R. Srinivasan, K.W. King, and S. Dagitz. 1997. SWAT User Manual. USDA-ARS, Temple, TX. In: http://www.brc.tamus.edu/swat/swatdoc.html#old

Brooks, R.H. and A.T. Corey. 1964. Hydraulic properties of porous media. Hydrology Paper #3, CSU, Fort Collins, CO.

Burman, R.D., P.R. Nixon, J.L. Wright, W.O. Pruitt. 1983. Water requirements. In Design and Operation of Farm Irrigation Systems, ASAE Monograph #3, American Society of Agricultural Engineers, St. Joseph, MI.

Campbell, G.C. and Norman, 1998. An Introduction to Environmental Biophysics. Springer-Verlag, New York.

Chow, V.T., D. R. Maidment, and L.W. Mays. 1987. Applied Hydrology. McGraw Hill.

Chu, S.T. 1978. Infiltration during an unsteady rain. Water Resources Research, Vol. 14(3): 461-466.

Elliot, W.J., A.M. Liebenow, J.M. Laflen and K.D. Kohl. 1989. A compendium of soil erodibility data from WEPP cropland soil field erodibility experiments 1987 & 1988. NSERL Report #3, The Ohio State University and USDA Agricultural Research Service, Columbus, OH.

Flanagan, D.C. and M.A. Nearing (eds). 1995. Hillslope Profile and Watershed Model Documentation. NSERL Report NO.10. West Lafayette.

Foster, G.R. 1982. Modeling the erosion process. In Hydrologic Modeling of Small Watersheds, Ed. Haan et al., ASAE Monograph #5, St. Joseph, MI.

Foster, G.R. and L.D. Meyer. 1972. A closed-form soil erosion equation for upland areas. In Sedimentation, Ed. Shen, Colorado State University, Fort Collins, CO.

Frederick, R. H., V. A. Myers, and E. P. Auciello. 1977. Five to 60 minute precipitation frequency for the Eastern and Central United States; NOAA Technical Memorandum NWS HYDRO-35.

Garen, D. C. and S.J. Burges. 1981. Approximate error bounds for simulated hydrograph. Journal of Hydraulics Division, Proc. ASCE, Vol. 107(HY11): 1519-1534.

Gray, D. H. and R. B. Sotir. 1996. Biotechnical and soil bioengineering slope stabilization: A practical guide for erosion control. John Wiley & Sons. Inc.

Haan, C.T., B.J. Barfield, and J.C. Hayes. 1994. Design Hydrology and Sedimentology for Small Watersheds. Academic Press, San Diego, California. pp. 49-51.

Hershfield, D.M. 1961. Rainfall Frequency Atlas of the United States for durations from 30 minutes to 24 hours and Return Periods from 1 to 100 Years; Technical Paper No. 40. Department of Commerce, Washington DC, May 1961.

Hjelmfelt, A.T. 1980. Curve number procedure as infiltration method. Journal of the Hydraulics Division, ASCE, Vol. 106(HY6): 1107 1111.

Holtan, H.N. 1961. A Concept for Infiltration Estimates in Watershed Engineering ARS 41-51, Agricultural Research Service, U.S. Department of Agriculture, pp 25.

Horton, R.E. 1939. Analysis of Runoff-Plat Experiments with Varying Infiltration-Capacity. Transactions of the American Geophysical Union:: 693-711.

Jensen, M.E., R.D. Burman, and R.G. Allen. 1990. Evapotranspiration and Irrigation Water Requirements. ASCE Manuals No. 70. ASCE, New York.

Jones, C.A., J.T. Ritchie, J.R. Kiniry, and D.C. Godwin. 1986. Subroutine structure. In CERES-Maize: A Simulation Model of Maize Growth and Development. Eds. C.A. Jones and J.R. Kiniry. Texas A&M University Press, College Station, TX.

Keifer, C.J. and H. H. Chu. 1957. Synthetic storm pattern for drainage design. Journal of the Hydraulics Division, Proc. ASCE, Paper 1332, Vol. 83 (HY 4): 1332- 1 to 1332-25.

Kent, KM. 1973. A Method for Estimating Volume and Rate of Runoff in Small Watersheds. USDA SCS-TP-149.. 1-19.

Larson, C.L. 1985. Modeling the effects of soil moisture on evapotranspiration. Hydrological Science and Technology, Vol. 1:7 11.

Lee, X.X. 1978. Forest Microclimatology. Columbia University Press, New York.

Li, R-M, M.A. Stevens, and D.B. Simons. 1976. Solutions to Green-Ampt Infiltration Equation Journal of the Irrigation and Drainage Divison, pp. 239-248.

Matalas, N.C. 1967. Mathematical assessment of synthetic hydrology. Water Resources Research, Vol. 3 (4): 937-945.

Mein, R.G. and C.L. Larson. 1973. Modeling infiltration during a steady rain. Water Resources Research, Vol. 9(2): 384 394.

Onstad, C. A. 1984. Depressional storage on tilled soil surfaces. Transactions of the ASAE, 729 732.

Press, W.H., B.P. Flannery, S.A. Teukolsky, and W.T. Vetterling. 1992. Numerical Recipies in C: Art of Scientific Computing. Cambridge Press.

Priestley, M.B. 1981. Spectral Analysis and Time Series. Academic Press, New York.

Soil Conservation Service. 1972. National Engineering Handbook, Section 4: Hydrology, USDA, Washington D.C.

Rawls, W.J., L.R. Ahuja, and D.L. Brakensiek. 1989. Estimating soil hydraulic properties from soils data. In Proceedings of the International Workshop on Indirect Methods for Estimating the Hydraulic Properties of Unsaturated Soils, Ed. van Genuchten, Leij and Lund: 329-340.

Richardson, C.W. 1981. Stochastic simulation of daily precipitation, temperature and solar radiation. Water Resources Research, Vol. 17(1): 182 190.

Ritchie, J. T., and E. Burnett. 1971. Dryland evaporative flux in a subhumid climate: II. Plant influnces. Agronomy Journal, Vol. 63: 56-62.

Ritchie, J.T. and E. Burnett 1971. Dryland evaporative flux in a subhumid climate. II. Plant influences. Agronomy Journal, Vol. 63: 56-62.

van Genuchten, M. Th. 1980. A closed-form equation for predicting the hydraulic conductivity of unsaturated soils. Soil Sci. Soc. Am. J., Vol. 44:892-898.

Williams, J.R. 1975. Sediment-yield prediction with universal equation using runoff energy factor. In Present and Prospective Technology for Predicting Sediment Yield and Sources, ARS-S 40: 244-251.

Wilson, B.N., B. J. Barfield and I. D. Moore. 1983. A Hydrology and Sedimentology Watershed Model. Part I: Modeling Techniques. Special Publication, Agricultural Engineering Department, University of Kentucky, Lexington, Kentucky.

Wilson, B.N., B. J. Barfield, I. D. Moore, and R. C. Warner. 1984. A hydrology and sedimentology watershed model. Part II: Sedimentology component. Trans. of ASAE 27(5):1378-1384.

Wilson, B.N. 1993. Development of a fundamentally based detachment model. Transactions of the ASAE, Vol. 36(4): 1105-1114.

Wilson, B.N. and M.G. Headrick. 1998. A rainfall hyetograph method for climate generation models. Presented at the 1998 ASAE Annual International Meeting, ASAE Paper 982022, 2950 Niles Road, St. Joseph, MI 49085-9659

Wilson, B.N. and J.W. Brown. 1992. Development and evaluation of a dimensionless unit hydrograph. Water Resources Bulletin, Vol. 28(2): 397-408.

Wilson, D.R. and P.D. Jamieson. 1984. Models of growth and water use of wheat in New Zealand. In Wheat Growth and Modeling, Eds. W. Day and R.K. Atkin, Plenum Press, New

York.

Wischmeier, W.H. and D.D. Smith. 1960. A universal soil-loss equation to guide conservation farm planning. Seventh International Congress of Soil Science, pp. 418-425.

Wischmeier, W.H. and D.D. Smith. 1965. Predicting rainfall-erosion losses from cropland east of the Rocky Mountains - A Guide for Selection of Practices for Soil and Water Conservation. Agricultural Handbook No. 282, U.S. Department of Agriculture.

Yang, C.T. 1973. Incipient motion and sediment transport. Proc. ASCE, Journal of Hydraulics Division, Vol. 99(HY10): 1805-1826.